Adaptive Virtual Waveform Design for Millimeter-Wave Joint Communication-Radar

Preeti Kumari, *Student Member, IEEE* Sergiy A. Vorobyov, *Fellow, IEEE*, and Robert W. Heath, Jr., *Fellow, IEEE*

***Abstract*—Joint communication and radar (JCR) waveforms with fully digital baseband generation and processing can now be realized at the millimeter-wave (mmWave) band. Prior work has developed a mmWave wireless local area network (WLAN)-based JCR that exploits the WLAN preamble for radars. The performance of target velocity estimation, however, was limited. In this paper, we propose a virtual waveform design for an adaptive mmWave JCR. The proposed system transmits a few non-uniformly placed preambles to construct several receive virtual preambles for enhancing velocity estimation accuracy, at the cost of only a small reduction in the communication data rate. We evaluate JCR performance trade-offs using the Cramér-Rao Bound (CRB) metric for radar estimation and a novel distortion minimum mean square error (MMSE) metric for data communication. Additionally, we develop three different MMSE-based optimization problems for the adaptive JCR waveform design. Simulations show that an optimal virtual (non-uniform) waveform achieves a significant performance improvement as compared to a uniform waveform. For a radar CRB constrained optimization, the optimal radar range of operation and the optimal communication distortion MMSE (DMMSE) are improved. For a communication DMMSE constrained optimization with a high DMMSE constraint, the optimal radar CRB is enhanced. For a weighted MMSE average optimization, the advantage of the virtual waveform over the uniform waveform is increased with decreased communication weighting. Comparison of MMSE-based optimization with traditional virtual preamble count-based optimization indicated that the conventional solution converges to the MMSE-based one only for a small number of targets and a high signal-to-noise ratio.**

I. Introduction

Millimeter-wave (mmWave) spectrum is an enabling technology to realize high data rate communication and high resolution radar sensing for many demanding applications, such as autonomous driving [3]. Traditional mmWave radars employ heavy analog pre-processing due to the use of low-speed analog-to-digital converters (ADC) and frequency-modulated continuous-wave (FMCW) technology [4]. While effective for initial implementations, analog designs are restrictive and limit the performance as well as flexibility for futuristic radar designs [5]. To address these concerns, mmWave communications hardware with high-speed ADCs can be leveraged to realize a mmWave radar system with fully digital time-domain baseband processing [6]. Further improvements can be achieved by combining radar and communication into a single joint mmWave system that uses a common waveform to enable hardware reuse. These new joint mmWave waveforms will provide advantages in terms of cost, size, power consumption, spectrum usage, and adoption of communication-capable vehicles.

The prior approaches on joint systems are mainly classified as either joint radar-communication (JRC) waveforms (i.e., radar-centric) or joint communication-radar (JCR) waveforms (i.e., communication-centric) [7]. With JRC waveforms, the communication messages are modulated on top of the radar waveforms, such as pulse position modulation in [8], phase modulation in [9], or continuous phase modulation in [10]. Additionally, the JRC waveforms have been realized by embedding communication information in the transmit beamforming vectors [11]. These waveforms, however, do not support high data rates as the communication signal must be spread to avoid disturbing the radar required properties. To achieve high spectral efficiency without complex equalization filters, most of the JCR systems at sub-6 GHz frequencies use orthogonal frequency-division multiplexing (OFDM) waveforms. The communication and radar performances are, however, limited due to the bandwidth available.

Recently, a number of mmWave wideband JCR waveforms have been proposed that leverages consumer wireless technologies [12]–[16]. In [12], a full-duplex IEEE 802.11ad-based radar was proposed that exploits the preamble of a single-carrier (SC) physical (PHY) layer frame to simultaneously achieve cm-level range resolution and Gbps data rates. A major limitation in [12] is that the performance of the velocity estimator was poor due to the short length of the preamble. In [13], an opportunistic radar was developed using an IEEE 802.11ad control PHY packet, which contains a longer preamble than SC PHY, for a single target scenario. Unfortunately, the probing signal duration is still small leading to poor velocity estimation, the data rate supported is at most 27.5 Mbps, and the update rate is very low. To enhance velocity estimation resolution, [14] investigated the possibility of increasing radar integration time by developing velocity estimation algorithms that exploit multiple fixed-length IEEE 802.11ad SC PHY frames. Similar velocity enhancement techniques were used in [15] that proposed an IEEE 802.11ad media access control configuration to accommodate radar operations for vehicle-to-infrastructure applications. In [16], an OFDM mmWave

Preeti Kumari and Robert W. Heath Jr. are with the Wireless Networking and Communications Group, the University of Texas at Austin, TX 78712-1687, USA (e-mail: {preeti_kumari, rheath}@utexas.edu). Sergiy A. Vorobyov is with the Aalto University, Konemiehentie 2, 02150 Espoo, Finland (email: sergiy.vorobyov@aalto.fi).

This research was partially supported by the U.S. Department of Transportation through the Data-Supported Transportation Operations and Planning (D-STOP) Tier 1 University Transportation Center, by the Texas Department of Transportation under Project 0-6877 entitled Communications and Radar-Supported Transportation Operations and Planning (CAR-STOP), and by the National Science Foundation under Grant No. ECCS-1711702 and CNS-1731658. This paper was presented in part at the IEEE ICASSP Conference, March 2017 [1] and at the IEEE ICASSP conference, April 2018 [2].

waveform was proposed for a bi-static automotive JCR system that also exploited preambles from multiple frames at a constant spacing for enhancing velocity estimation performance. The approaches in [14]–[16], however, require increasing the total preamble duration to achieve desirable high-accuracy velocity estimation, which would incur degradation in the communication data rate.

In this paper, we use sparse sensing techniques in the time domain to optimize the trade-off between communication and radar performance for the waveform design of a JCR system. We exploit the preamble of a communication frame as a radar pulse. The radar pulses are placed in a non-uniform fashion by varying the frame lengths, and their locations form a restricted difference basis [17]. Then, we use a few non-uniformly placed pulses in a coherent processing interval (CPI) to construct a virtual difference co-waveform with several uniform virtual preambles. This virtual increase in the radar pulse integration time enables enhanced velocity estimation at a given communication rate as compared to a uniform waveform [14]. The virtual pulse approach is conceptually similar to the staggered pulse repetition intervals (PRI) used in the classical long-range radar [18, Ch. 17] and sparse sampling/arrays used in the undersampled frequency/angle/channel estimation [17], [19], [20]. Most of the existing sparse sensing approaches are focused on optimizing the sparse antenna array configurations by maximizing the antenna aperture for a given number of antenna elements. In this paper, however, we design a virtual JCR waveform using a novel minimum mean square error (MMSE)-based optimization that accurately quantifies the trade-off between communication and radar performance.

We make the following key assumptions in our proposed mmWave JCR waveform design. First, we assume that the location and relative velocity of a target remain constant during a CPI. This is justified by the small enough acceleration and velocity of a target relative to the radar sensor, as found in automotive applications [21]. Second, we assume full-duplex radar operation due to the recent development of systems with sufficient isolation and self-interference cancellation [22], [23]. Third, we assume perfect data interference cancellation on the training part of the received JCR waveform because the transmitted data is known at the radar receiver. These assumptions are explained in more detail in Section II.

The main contributions of this paper are summarized as follows.

- We propose a novel formulation for a wideband JCR system that transmits virtual waveform at the mmWave band. This formulation captures the nuances of the frequency-selective sparse mmWave channel description for both communication and radar systems. Additionally, we develop a generic virtual JCR waveform structure in the system model that can be further tuned to achieve optimal JCR performance using sparse sensing techniques.
- We develop a novel effective distortion minimum mean square error (DMMSE) metric for communication that is comparable with the radar Cramér-Rao bound (CRB) metric for velocity estimation. The MMSE-based metrics enable us to accurately quantify the trade-off between communication and radar systems.
- We formulate three different optimization problems for designing an adaptive JCR waveform that meets the Pareto-optimal bound. The first one minimizes the radar CRB under the constraint of a minimum communication DMMSE. The second one minimizes the communication DMMSE for a given minimum radar CRB. The third one considers a more flexible weighted average of communication and radar performance for the JCR system.
- We solve the proposed JCR optimization problems for a uniform waveform and for virtual waveforms that can be represented in closed-form and contain no holes in their corresponding difference co-waveforms, such as nested virtual waveforms or Wichmann virtual waveforms. The use of specific virtual waveform configurations reduces the computational complexity for finding the optimal JCR waveform design.
- We carry out simulations to study the performance trade-offs in the JCR waveform design and compare the optimal performances achieved by different JCR waveform solutions. We explore the effects of signal-to-noise ratio (SNR), the number of preambles used, and the number of radar targets on the virtual waveform design. The simulation parameters are based on automotive applications and the IEEE 802.11ad-based standard. The results suggest that virtual waveforms are highly desirable at high SNR with low target density (i.e., a small ratio of target count to the number of preambles) and at low SNR with high communication DMMSE. Comparison of MMSE-based optimization with more traditional virtual preamble (VP) count-based optimization indicates that the traditional solution converges to the MMSE-based one only at low target density and high SNR.

The work in this paper is a significant extension of our previous conference contributions [1], [2]. In addition to a detailed exposition on the adaptive JCR waveform design, we have included a multi-target radar model and a frequency-selective communication channel model for demonstrating the superiority of virtually placed preambles as compared to uniformly placed preambles.

The rest of the paper is organized as follows. We formulate an integrated model for our proposed JCR system in Section II. For the proposed system, we develop a radar processing technique in Section III. Then, we describe the performance metrics and the associated trade-off for the JCR waveform design in Section IV. In Section V, we develop three optimization problems for the adaptive JCR waveform design. In Section VI, we outline the main idea of virtual waveform design and different specific solution approaches for waveform optimization. We describe the simulation results and performance evaluations in Section VII. Finally, we conclude our work and provide directions for future work in Section VIII.

Notation: We use the following notation throughout the paper: The notation $\mathcal{N}_{\mathcal{C}}(u, \sigma^2)$ is used for a complex Gaussian random variable with mean u and variance σ^2. The projection matrix onto the null space of matrix $\mathbf{A}$ is defined as $\mathbf{\Pi}_{\mathbf{A}}^{\perp} = \mathbf{I} - \mathbf{A}(\mathbf{A}^*\mathbf{A})^{-1}\mathbf{A}^*$. The operators $|\cdot|$ represents the cardinality of a matrix, $\mathrm{Conv}\,(\cdot)$ denotes the convex hull, and $\mathrm{Tr}\,[\cdot]$ indicates the trace of a square matrix. The notation $(\cdot)^{\mathrm{T}}$,

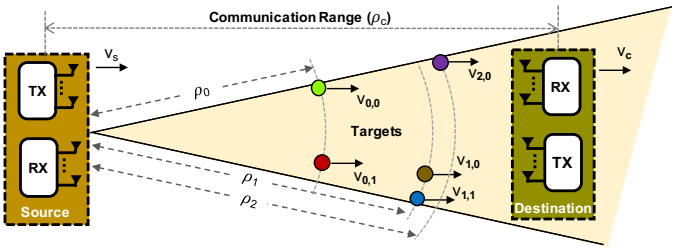

Fig. 1. The source sends a mmWave waveform to the destination receiver and uses the echoes from multiple moving targets (including the destination) to estimate their ranges $\{\rho_\ell\}_{\ell=0}^{L-1}$ and velocities $\{v_{\ell,k}\}_{\ell=0,k=0}^{L-1,K-1}$.

$(\cdot)^*$, and $(\cdot)^{\rm c}$ stand for transpose, Hermitian transpose, and conjugate of a matrix/vector, while $(\cdot)^{-1}$ represent the inverse of a square full-rank matrix. Additionally, $\mathrm{vec}(\cdot)$ vectorizes a matrix to a long vector, $\mathrm{diag}(\cdot)$ forms a vector into a diagonal matrix, while $\odot$ and $\otimes$ represent Khatri-Rao and Kronecker product of matrices.

II. System Model

In this section, we formulate transmit (TX) and receive (RX) signal models for the proposed adaptive mmWave JCR system, as illustrated in Fig. 1. We consider the case where a full-duplex source transmits the JCR waveform at a carrier wavelength λ to a destination receiver at a distance $\rho_{\rm c}$ moving with a relative velocity $v_{\rm c}$, while simultaneously receiving echoes from the surrounding moving targets. First, we propose an adaptive single-carrier mmWave waveform structure that serves as the TX signal at the source for both communication and radar systems simultaneously. Then, we develop RX signal models for the communication receiver at the destination and the radar receiver at the source for the frequency-selective channels.

A. Transmit signal model

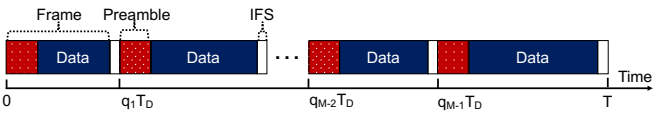

Fig. 2. A CPI of T seconds duration with M JCR frames. Each frame contains a fixed-length preamble of P symbols, a varying length data segment, and an inter-frame space (IFS) of constant duration. The length of each frame is an integer multiple, q_m, of the Nyquist sampling interval in the Doppler domain, $T_{\rm D}$.

We consider a generic TX waveform structure with μ fraction of communication symbols and $(1-\mu)$ fraction of preamble symbols in a CPI of T seconds with M frames. Each frame consists of a fixed preamble duration, $PT_{\rm s}$, and a variable data length, which leads to a varying frame length as shown in Fig. 2. The IEEE 802.11ad standard can realize this multi-frame approach using the block/no acknowledgment policy during the communication between a dedicated pair of nodes in the data transmission interval [24, Ch. 9]. To unambiguously estimate a maximum relative target velocity $v_{\max}$ in a CPI, the $m^{\rm th}$ frame is considered to be located at an integer multiple, q_m, of the Doppler Nyquist sampling interval, $T_{\rm D} \leq \lambda/(4v_{\max})$.

We denote the unit energy TX pulse-shaping filter as $g_{\rm TX}(t)$, the signaling bandwidth as W, and the symbol period as $T_{\rm s} \approx 1/W$. The transmitted symbol sequence corresponding to the $m^{\rm th}$ frame with N_m symbols is denoted by $s_m[n]$, which satisfies the average power constraint $\mathbb{E}\left[|s_m[n]|^2\right] = \mathcal{E}_{\rm s}$. Then, the generic complex-baseband continuous-time representation of the single-carrier TX waveform in a CPI is given as

$$x(t) = \sum_{m=0}^{M-1} \sum_{n=0}^{N_m-1} s_m[n] g_{\rm TX}(t - nT_{\rm s} - q_m T_{\rm D}). \quad (1)$$

The generic TX waveform parameters, such as the location and size of the $m^{\rm th}$ frame, can be further optimized to achieve desirable JCR performance as described in Section V.

In this paper, we consider a single data stream model that supports analog beamforming with frequency flat TX/RX beam steering vectors [14]. We assume that the source and destination align their beams toward each other with line-of-sight (LoS) frequency-selective communication and radar channel. The insights and analysis of this work can also be extended to mmWave multiple-input-multiple-output (MIMO) radar research using low-resolution ADCs [25] by focusing on the signal model for a given angular bin. We will now formulate the JCR received signal model after the TX/RX beamforming for multiple frames in a CPI.

B. Receive signal models

We consider a dwell time consisting of $N_{\rm CPI}$ coherent processing intervals. During the dwell time, we assume that the acceleration and the relative velocity of a moving target is small enough to assume constant velocity and that the target is quasi-stationarity (constant location parameters). We assume a frequency-selective Rayleigh fading model for both communication and radar channels during the dwell time for simplicity. This work can also be extended for a general Ricean fading mmWave channel model with block sparsity by deriving corresponding CRB bounds for different Ricean fading factors that lies between zero (Rayleigh fading) and infinity (no fading). In each of the CPIs with M frames, we consider a block fading model that assumes a constant channel gain for each delay tap.

1) Communication received signal model: For evaluating the trade-off between communication and radar performance, we model the communication signal received at a distance $\rho_{\rm c}$. Assuming a highly directional mmWave LoS communication link is established between the source and destination, the large-scale path-loss $G_{\rm c}$ is given as [26]

$$G_{\rm c} = \frac{G_{\rm TX} G_{\rm RX} \lambda^2}{(4\pi)^2 \rho_{\rm c}^{\rm PL}}, \quad (2)$$

where PL is the path-loss exponent, $G_{\rm TX}$ is the TX array gain, and $G_{\rm RX}$ is the RX array gain.

After TX/RX beamforming, symbol synchronization, and frequency synchronization, the received communication signal is a sum of the contributions from $L_{\rm c}$ delayed and attenuated copies of the transmitted signals as well as the additive white Gaussian noise (AWGN) with zero mean and variance $\sigma_{\rm n}^2$. The small-scale complex gain of the $\ell^{\rm th}$ channel delay path, $\alpha_{\rm c}[\ell]$,

is assumed to be independently and identically distributed (IID) $\mathcal{N}_{\mathcal{C}}(0, \sigma_{\rm c}^2[\ell])$, where $\sigma_{\rm c}^2[\ell]$ represents the average tap power normalized such that $\sum_{\ell=0}^{L_{\rm c}-1} \sigma_{\rm c}^2[\ell] = 1$. Therefore, the communication RX signal $y_{{\rm c},m}[n]$ corresponding to the $n^{\rm th}$ symbol in the $m^{\rm th}$ frame with noise $w_{{\rm c},m}[n]$ is

$$y_{{\rm c},m}[n] = \sqrt{G_{\rm c}} \sum_{\ell=0}^{L_{\rm c}-1} \alpha_{\rm c}[\ell] s_m[n-\ell] + w_{{\rm c},m}[n]. \quad (3)$$

The communication SNR is defined as $\zeta_{\rm c} \triangleq \mathcal{E}_{\rm s} G_{\rm c}/\sigma_{\rm n}^2$.

2) Radar received signal model: We represent the doubly selective (time- and frequency-selective) mmWave radar channel obtained after TX/RX beamforming using the virtual representation obtained by uniformly sampling in the range dimension [14]. We assume that there are L range bins. The $\ell^{\rm th}$ range bin is assumed to consist of a few, $K[\ell]$, virtual scattering centers with different velocities. Each of the $(\ell,k)^{\rm th}$ virtual scattering center is characterized by its distance $\rho[\ell]$, delay $\tau[\ell]$, velocity $v_k[\ell]$, Doppler shift $\nu_k[\ell] = 2v_k[\ell]/\lambda$, and radar cross-section $\sigma_{{\rm RCS},k}[\ell]$. The channel gain, $\beta_k[\ell]$, corresponding to the $(\ell,k)^{\rm th}$ virtual target scattering center is (as used extensively in previous work, e.g., [27])

$$\beta_k[\ell] = \frac{G_{\rm TX} G_{\rm RX} \lambda^2 \sigma_{{\rm RCS},k}[\ell]}{64\pi^3 \rho^4[\ell]} \quad (4)$$

and is assumed IID $\mathcal{N}_{\mathcal{C}}(0, G_k[\ell])$.

After matched filtering (MF) with the RX pulse shaping filter $g_{\rm RX}(t)$ and symbol rate sampling, the received radar signal is a sum of the contributions from the attenuated, delayed, Doppler-shifted, and sampled MF echoes as well as the AWGN with zero mean and variance $\sigma_{\rm n}^2$. Therefore, the radar received signal model corresponding to the $m^{\rm th}$ frame with the net TX-RX pulse shaping filter $g(t) = g_{\rm TX}(t) * g_{\rm RX}(t)$, delayed and sampled MF echo from the $\ell^{\rm th}$ range bin $\varepsilon_m[n,\ell] = \sum_{i=0}^{N_m-1} s_m[i] g((n-i)T_{\rm s} - q_m T_{\rm D} - \tau[\ell])$ and noise $w_{{\rm r},m}[n]$ is given as

$$y_m[n] = \sum_{\ell=0}^{L-1} \varepsilon_m[n,\ell] \sum_{k=0}^{K[\ell]-1} \sqrt{\beta_k[\ell]} {\rm e}^{-{\rm j}2\pi\nu_{\ell,k}(nT_{\rm s}+q_m T_{\rm D})} + w_{{\rm r},m}[n]. \quad (5)$$

The received echo $y_m[n]$ is comprised of reflections corresponding to the TX symbol $s_m[n]$ as well as an intersymbol interference from the other TX symbols that depends on the choice of the TX/RX pulse shaping filters and the doubly-selective radar channel parameters.

We use the training sequences for radar parameter estimation due to to their good correlation properties. The training part might incur some interference from the data part because of the larger delay spread observed in the two-way radar channel as compared to the guard interval employed between the preamble and the data part in a typical communication system. Motivated by the recent development of non-orthogonal multiple access techniques with successive interference cancellation [28], we assume perfect cancellation of the data part on the received training signal. Developing and evaluating algorithms to cancel the communication data interfence while receiving the radar segment reflection is a subject of future work.

We assume the channel to be time invariant within the preamble duration of a single frame due to slow enough velocity and small enough preamble duration. Therefore, the received signal model corresponding to the training part with $\varepsilon_{\rm t}[n,\ell]$ as the preamble/training part of $\varepsilon[n,\ell]$ that remains same for each frame is

$$y_m^{\rm t}[n] = \sum_{\ell=0}^{L-1} \varepsilon_{\rm t}[n,\ell] \sum_{k=0}^{K[\ell]-1} \sqrt{\beta_k[\ell]} {\rm e}^{-{\rm j}2\pi\nu_k[\ell] q_m T_{\rm D}} + w_{{\rm r},m}[n]. \quad (6)$$

Note that the virtual channel model with $\sum_{\ell=0}^{L-1} K[\ell]$ scattering centers is used in (6).

III. Proposed Radar Processing

In this section, we propose a radar processing technique for estimating target velocities using the proposed JCR frames of the same or varying lengths. The radar processing technique exploits the preamble part of the JCR frame that consists of training sequences with good auto-correlation properties, such as Golay complementary sequences used in the IEEE 802.11ad-based automotive radar applications [13], [14]. First, we estimate the channel using a typical communication-based preamble processing algorithm that exploits the correlation properties of the training sequences [14]. Then, we calculate the target velocities from the estimated channel using super-resolution velocity estimation algorithms.

Denoting $b_k[\ell] \triangleq \gamma\sqrt{\mathcal{E}_{\rm s}\beta_k[\ell]}$ as signal amplitude in the channel, γ as the integration gain due to the correlation-based channel estimation, $w_m[\ell]$ as the noise in the channel, and $u_k[\ell] \triangleq \nu_k[\ell] T_{\rm D}$ as the discrete Doppler frequency, the channel corresponding to the detected target in the $\ell^{\rm th}$ range bin that is derived using the $m^{\rm th}$ frame received in (6) is given as

$$h_m[\ell] = \sum_{k=0}^{K[\ell]-1} b_k[\ell] {\rm e}^{-{\rm j}2\pi u_k[\ell] q_m} + w_m[\ell], \quad (7)$$

where $w_m[\ell]$ is distributed as $\mathcal{N}_{\mathcal{C}}(0, \sigma_n^2)$. The channel vector corresponding to the $\ell^{\rm th}$ range bin for a CPI of M frames is $\mathbf{h}[\ell] \triangleq [h_0[\ell], h_1[\ell], \cdots, h_{M-1}[\ell]]^{\rm T}$.

The focus of this paper is on target velocity estimation. Therefore, we describe algorithms for estimating the velocity of a single target in a specific range bin, say ℓ_0, which can be similarly performed for other range bins. To simplify the expressions, we henceforth omit the notation ℓ denoting the range bin (e.g., $b_k[\ell]$ becomes just b_k).

Denoting the channel signal amplitude vector $\mathbf{b} \triangleq [b_0, b_1, \cdots, b_{K-1}]^{\rm T}$, the channel Doppler vector corresponding to the $k^{\rm th}$ velocity, $\mathbf{d}(v_k) \triangleq [1, e^{j2\pi u_k q_1}, \cdots, e^{j2\pi u_k q_{M-1}}]^{\rm T}$, the channel Doppler matrix $\mathbf{D} \triangleq [\mathbf{d}(v_0), \mathbf{d}(v_1), \cdots, \mathbf{d}(v_{K-1})]$, and the channel noise vector $\mathbf{w} \triangleq [w_0, w_1, \cdots, w_{K-1}]^{\rm T}$, the channel vector corresponding to the range bin ℓ_0 with $K > 0$ detected targets is given by

$$\mathbf{h} = \mathbf{D}\mathbf{b} + \mathbf{w}. \quad (8)$$

This channel vector is used for target velocity estimation.

Due to space limitations and for simplicity of our basic study here, we focus on subspace methods, in particular on

the class of multiple signal classification (MUSIC) techniques, for velocity estimation algorithms among many possible approaches [29]–[31]. The velocity resolution obtained by the subspace methods is not constrained by the duration of the CPI as in the fast Fourier transform (FFT)-based technique used in [14]. Therefore, a subspace method can provide higher resolution in the mobile environment with limited CPI. Subspace-based velocity estimation using multiple preambles in a CPI can be performed by exploiting sample covariance matrix of the channel in (8) [29]–[31]. The covariance matrix of the channel with $p_k = \mathbb{E}\left[b_k b_k^*\right]$ as the power of the k^{th} target and $\mathbf{P} \triangleq \text{diag}(p_0, p_1, \cdots, p_{K-1})$ as the target covariance/power matrix is given by

$$\mathbf{R} = \mathbf{DPD}^* + \sigma_{\text{n}}^2 \mathbf{I}. \tag{9}$$

We define the SNR of the received radar signal at the source vehicle corresponding to the k^{th} target as $\zeta_{\text{r}}[k] = p_k/\sigma_{\text{n}}^2$.

We evaluate the CRB performance metric for the velocity estimation performance of the subspace method using the channel covariance matrix in (9), as described in Section IV. In Section VI, we further illustrate the MUSIC-based velocity estimation algorithms for specific waveform design solutions that exploits the finite snapshot version of (9).

IV. Performance Metrics

In this section, we first describe the spectral efficiency performance metric for communication systems and the CRB performance metric for radar systems. Then, we describe a novel metric for assessing the system trade-off between radar and communication for a joint waveform design.

A. Communication performance metric

The channel capacity for the received communication signal in (3) with eigenvalues of the channel matrix as $\{\lambda_{\text{c}}[n]\}_{n=1}^N$, fraction of data symbols $\mu = 1$, data power coefficients $\{\xi[n]\}_{n=1}^N$ satisfying $\frac{1}{N}\sum_{n=1}^N \xi[n] = 1$, data symbol $s[n] \sim \mathcal{NC}(0, \xi[n]\mathcal{E}_{\text{s}})$, and noise $w_{\text{c}}[n] \sim \mathcal{NC}(0, \sigma_{\text{w}}^2)$ is obtained by allocating optimum power based on the vector coding among a block of $N \to \infty$ symbols of the single-carrier waveform [32, Ch. 4]. The maximum communication spectral efficiency achieved using vector coding transmission for $N \to \infty$ is expressed as

$$r = \frac{1}{N}\sum_{n=1}^{N} \log_2\left(1 + \zeta_{\text{c}}\lambda_{\text{c}}[n]\xi[n]\right) \ \text{ bits/s/Hz} \tag{10}$$

and the channel capacity in bits per second (bps) is given as $C = Wr$. Note that the achievable spectral efficiency of a communication system depends on the implemented precoder and equalizer [33], [34], and are all upper bounded by (10) for $N \to \infty$.

When $\mu \leq 1$ fraction of communication symbols are transmitted in a CPI with the channel capacity C, we define the effective communication data rate as $C_{\text{eff}} = \mu C$, as in [32, Ch. 7]. Additionally, we can define the effective communication spectral efficiency for $\mu \leq 1$ as

$$r_{\text{eff}} = \mu r = \frac{\mu}{N}\sum_{n=1}^{N} \log_2\left(1 + \zeta_{\text{c}}\lambda_{\text{c}}[n]\xi[n]\right) \ \text{ bits/s/Hz}, \tag{11}$$

which satisfies $C_{\text{eff}} = Wr_{\text{eff}}$ bps when $N \to \infty$.

B. Radar performance metric

The CRB is a lower bound on the variance of an unbiased estimator, and is widely employed as a performance criterion for direction-of-arrival and velocity estimations [35]–[38]. The aperture is another commonly employed metric for evaluating the performance of the sparse sensor array/sampling configurations for a given number of antenna elements/samples [17], [19], [39]. In contrast to the aperture metric or the equivalent VP count for virtual waveform design, the multi-target CRB takes into account both the mainlobe and sidelobes of the ambiguity function. It also captures the saturation effects observed in virtual waveforms at high SNR. In addition, it reflects the conditions for the nonexistence of unbiased estimators with finite variance, while other above mentioned commonly used metrics do not have such advantages. Additionally, the closed-form expression for the radar CRB metric is known in the existing literature [31], [37], [40], which offers analytical insights into the design of JCR waveforms. For white Gaussian noise, the CRB is also a lower bound on the MMSE for radar parameter estimation and is used for asymptotic analysis.

To express the CRB corresponding to (9) with η snapshots, we denote the derivative of the channel Doppler matrix $\mathbf{D}$ with respect to the K velocity parameters $\{v_k\}_{k=1}^K$ as $\dot{\mathbf{D}}$, the co-waveform Doppler matrix $\mathbf{D}_{\text{q}} \triangleq \mathbf{D}^{\text{c}} \odot \mathbf{D}$, the derivative of the co-waveform Doppler matrix as $\dot{\mathbf{D}}_{\text{q}} \triangleq \dot{\mathbf{D}}^* \odot \mathbf{D} + \mathbf{D}^* \odot \dot{\mathbf{D}}$, identity vector $\mathbf{i} \triangleq \text{vec}(\mathbf{I})$. Then, the CRB matrix for the K estimated velocities with $\mathbf{E} \triangleq (\mathbf{R}^{\text{T}} \otimes \mathbf{R})^{-1/2}\dot{\mathbf{D}}_{\text{q}}\mathbf{P}$ and $\mathbf{F} \triangleq (\mathbf{R}^{\text{T}} \otimes \mathbf{R})^{-1/2}[\mathbf{D}_{\text{q}} \quad \mathbf{i}]$ is [31]

$$\text{CRB} = \frac{1}{\eta}\left(\mathbf{E}^* \mathbf{\Pi}_{\mathbf{F}}^{\perp} \mathbf{E}\right)^{-1}. \tag{12}$$

Note that when the Fisher information matrix is necessarily singular, the CRB does not exist implying that no unbiased estimator with finite variance exists [41]. Additionally, the use of multiple snapshots can be achieved by using multiple CPIs within a dwell time. The number of available snapshots for estimating target velocities within a given range bin depends on the dwell time, where the quasi-stationarity (constant location and velocity parameters) assumption holds. It also depends on the latency desired for radar parameter estimation. The maximum number of available snapshots, however, can be increased by incorporating a range drift correction algorithm using tracking or technique similar to the range cell migration correction algorithm used in synthetic aperture radar systems [42, Ch. 6].

C. Joint communication-radar performance metric

In this section, we develop a novel JCR metric to quantify the trade-off between the radar and the communication performance. In [43], a range estimation rate metric for radar was proposed and is analogous to the data rate used in communication systems. The radar estimation, however, is not drawn from a countable distribution similar to communication data symbols. Therefore, the estimation rate metric is not an accurate representation of radar performance. The

derivation of estimation rate for radar round-trip delay is also not easily extendable to other radar parameters because several underlying simplifications made in [43], [44] may become invalid for the estimation of these other parameters [45]. Additionally, the number of radar performance metrics (e.g., range/velocity/direction of multiple targets, number of detectable targets, probability of detection and false alarm, range/velocity/angular resolution) that depend on μ is much larger than the few performance metrics used in communication. Therefore, instead of deriving equivalent estimation or information rates for each of these radar parameters in different scenarios, as in [45], we propose an effective communication DMMSE metric similar to a radar CRB performance metric.

To formulate an effective scalar communication metric, which parallels the concept of the radar CRB for JCR waveform design optimization, we propose an MMSE-based communication metric analogous to the distortion metric in the rate-distortion theory [46, Ch. 10]. The MMSE of a communication system with net spectral efficiency r, $\mu = 1$, and n^{th} spectral efficiency $r_n = \log_2(1+\zeta_{\text{c}}\lambda_{\text{c}}[n]\xi[n])$ in (11) is given as [47]

$$\begin{aligned}\text{MMSE}_{\text{c}} &\triangleq \mathbb{E}\left[(\mathbf{s}-\hat{\mathbf{s}})((\mathbf{s}-\hat{\mathbf{s}}))^*\right] \\ &= \text{diag}\big(2^{-r_1},\cdots,2^{-r_N}\big),\end{aligned} \tag{13}$$

where $\mathbf{s} = [s[1], s[2], \cdots s[N]]^{\text{T}}$ is the true TX symbol vector and $\hat{\mathbf{s}}$ is the MMSE estimated vector of $\mathbf{s}$.

Using (10) and (13), the relationship between MMSE_{c} and r becomes

$$\frac{1}{N}\text{Tr}\left[\log_2 \text{MMSE}_{\text{c}}\right] = -r. \tag{14}$$

Therefore, the effective communication DMMSE that satisfies

$$\frac{1}{N}\text{Tr}\left[\log_2 \text{DMMSE}\right] = -r_{\text{eff}} = -\mu \cdot r \tag{15}$$

is given as

$$\text{DMMSE} = \text{MMSE}_{\text{c}}^{\mu}. \tag{16}$$

The effective DMMSE derived for a single-target scenario in [1] also follows relations similar to (15) and (16). Note that determinant and largest eigenvalues could be used instead of trace in (15). Indeed, the determinant is a volume, the largest eigenvalue is the length along the longest axis, and the trace is a sum of all the eigenvalues. Therefore, the trace is a reasonable selection for a MMSE-based JCR performance metric. The performance trade-off between communication and radar can then be quantified in terms of the following scalar quantities: $\frac{1}{N}\text{Tr}\left[\log \text{DMMSE}\right]$ and $\frac{1}{K}\text{Tr}\left[\log \text{CRB}\right]$. Since the communication DMMSE and the radar CRB values are usually substantially different, the log-scale is used to achieve proportional fairness (PF) similar to the problem of resource allocation in multi-user communication [32, Ch. 7].

V. Adaptive Waveform Design Problem Formulation

In this section, we formulate an adaptive JCR waveform design to optimize the number of preambles M and the preamble locations $\{q_m\}_{m=1}^{M-1}$. The JCR performance optimization problem is a multi-objective (two-objective) problem of simultaneously optimizing both the radar performance, in terms of, for example, minimizing the velocity CRB, and the communication performance, in terms of minimizing the effective communication DMMSE. We can see from (15) that the communication MMSE metric denoted as $\frac{1}{N}\text{Tr}\left[\log \text{DMMSE}\right]$ is linear with respect to optimization variables M and $\{q_m\}_{m=1}^{M-1}$. The radar MMSE metric denoted as $\frac{1}{K}\text{Tr}\left[\log \text{CRB}\right]$ in (12), however, can be non-convex with respect to the optimization variables, as illustrated later in Section VII. Therefore, the region of achievable JCR objective values with the radar CRB and communication DMMSE pairs corresponding to the feasible values of preamble count and locations can be non-convex. Then, the optimal JCR performance is achieved by using the Pareto set of the minimum convex set (termed the convex hull) of the feasible non-convex JCR achievable objective values region, thereby enhancing at least radar CRB metric without degrading the communication DMMSE metric, similar to multi-user communication rate optimization [46, Ch. 15]. Additionally, the convex solution is achievable by using time-sharing or probabilistic occurrence techniques on the extreme points of the convex hull [48].

The scalarization approach is known to achieve a Pareto optimal point for multiple convex objectives [49, Ch. 4]. Therefore, the JCR performance optimization can be formulated as the weighted average of a convex hull of communication and radar MMSE-based performance metrics. Denoting the scalar communication DMMSE metric as $\varphi_{\text{c}}(\text{DMMSE}) \triangleq \frac{1}{N}\text{Tr}\left[\log \text{DMMSE}\right]$ and the scalar radar CRB metric as $\varphi_{\text{r}}(\text{CRB}) \triangleq \text{Conv}\left(\frac{1}{K}\text{Tr}\left[\log \text{CRB}\right]\right)$, which incorporates the convex hull operation with respect to the optimization variables, the JCR performance optimization problem can be formulated as

$$\begin{aligned}\underset{M,\{q_m\}_{m=1}^{M-1}}{\text{minimize}} \quad & \omega_{\text{r}}\varphi_{\text{r}}(\text{CRB}) + \omega_{\text{c}}\varphi_{\text{c}}(\text{DMMSE}) \\ \text{subject to} \quad & \{T, K, \rho\} = \text{constants}, \\ & 0 < q_1 < \cdots < q_{M-1} < T/T_{\text{D}},\end{aligned} \tag{17}$$

where $\omega_{\text{r}} \geq 0$ and $\omega_{\text{c}} \geq 0$ are the normalizing and weighting factors assigning the priorities for radar and communication tasks, respectively. Note that the weights can be adjusted adaptively with respect to the requirements imposed by different scenarios, such as varying radar SNR.

Alternatively, problem (17) can be modified as a minimization of one of the objectives with the second one written as a constraint that would guarantee an acceptable performance for one of the tasks. The radar CRB constrained formulation with a minimum required CRB Υ_{r} can be expressed as

$$\begin{aligned}\underset{M,\{q_m\}_{m=1}^{M-1}}{\text{minimize}} \quad & \varphi_{\text{c}}(\text{DMMSE}) \\ \text{subject to} \quad & \varphi_{\text{r}}(\text{CRB}) \leq \Upsilon_{\text{r}}, \\ & \{T, K, \rho\} = \text{constants}, \\ & 0 < q_1 < \cdots < q_{M-1} < T/T_{\text{D}}.\end{aligned} \tag{18}$$

The optimization in (18) simplifies to finding the minimum number of frames M that meets the required radar CRB value, whenever a specific sparse pulse configuration, such as coprime pulses, is assumed.

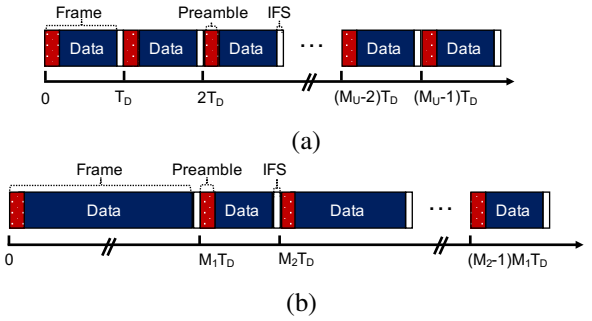

Fig. 3. Different virtual waveforms: (a) Uniform one, where a CPI consists of $M_{\rm U}$ equi-spaced frames of duration $T_{\rm D}$. (b) Coprime one, where a CPI consists of non-uniformly placed $M_{\rm V} = M_1 + M_2$ frames.

The communication DMMSE-constrained formulation with minimum required DMMSE $\Upsilon_{\rm c}$ is given by

$$\begin{aligned} \underset{M,\{q_m\}_{m=1}^{M-1}}{\text{minimize}} \quad & \varphi_{\rm r}(\text{CRB}) \\ \text{subject to} \quad & \varphi_{\rm c}(\text{DMMSE}) \leq \Upsilon_{\rm c}, \\ & \{T, K, \rho\} = \text{constants}, \\ & 0 < q_1 < \cdots < q_{M-1} < T/T_{\rm D}. \end{aligned} \tag{19}$$

The optimization in (19) for a constant predefined number of frames M for a large enough CPI T simplifies to the optimization of frame locations.

VI. Adaptive Waveform Design Solutions

Finding optimal virtual waveform designs as the solutions of the JCR optimization problems proposed in Section V is computationally difficult (generally has combinatorial complexity). To ensure polynomial complexity for solving the JCR optimization problems and for mathematical tractability, we use specific configurations of preamble locations that have good ambiguity functions. It helps to dramatically reduce the optimization complexity and problem size to only a few variables depending on the specific configurations used. In this section, we present different adaptive single-carrier waveform designs based on the JCR optimization problem formulations along with their associated algorithms. These solutions are mainly classified as uniform or non-uniform (virtual) waveform designs. In the uniform waveform (UW) design, the preambles are placed at a Doppler Nyquist rate $1/T_{\rm D}$, whereas in the non-uniform waveform design, the preambles are placed at a Doppler sub-Nyquist rate $1/(q_m T_{\rm D})$ with integer $q_m > 1$.

A. Uniform waveform design

In this approach, multiple frames, $M_{\rm U}$, are placed at a constant Doppler Nyquist sampling interval, $T_{\rm D}$, in a CPI of $T \geq M_{\rm U} T_{\rm D}$ seconds [14], as shown in Fig. 3(a). The $m^{\rm th}$ frame in a CPI is located at $q_m = m$ and the set of all preamble locations in a CPI is $\mathcal{M}_{\rm U} = \{1, 2, \cdots, M_{\rm U}\}$. Therefore, the weighted average formulation in (17) can be modified after incorporating the UW structure into the problem formulation as:

$$\begin{aligned} \underset{M_{\rm U}}{\text{minimize}} \quad & \omega_{\rm r}\varphi_{\rm r}(\text{CRB}) + \omega_{\rm c}\varphi_{\rm c}(\text{DMMSE}) \\ \text{subject to} \quad & \{T, K, \rho\} = \text{constants}, \\ & q_m = m \leq T/T_{\rm D} \quad \forall m = 1, 2, ..., M_{\rm U}. \end{aligned} \tag{20}$$

The other constrained optimization formulations in (18) and in (19) can be similarly modified by incorporating the uniform waveform structure into the formulations.

For the uniform waveform design, the CRB expression in (12) can be further simplified as [50]

$$\text{CRB} = \frac{\sigma_{\rm n}^2}{2\eta} \left\{ \text{Re}(\dot{\mathbf{D}}^* \mathbf{\Pi}_{\mathbf{D}}^{\perp} \dot{\mathbf{D}}) \odot (\mathbf{P}\mathbf{D}^* \mathbf{R} \mathbf{D} \mathbf{P})^{\rm T} \right\}^{-1}, \tag{21}$$

where CRB exists when the target count K is smaller than the number of preambles $M_{\rm U}$. As SNR goes to infinity, CRB in (21) reduces to zero [50]. Additionally, the radar CRB metric $\varphi_{\rm r}(\text{CRB})$ is convex with respect to $M_{\rm U}$ for uniform waveform, as illustrated later in Section VII. We use the standard MUSIC algorithms, which is asymptotically efficient, for estimating velocity using uniform waveforms when $K < M_{\rm U}$ [51].

The feasibility and behavior of optimal solutions in the waveform design problem formulations in (17), (18), and (19) depends on the velocity CRB in (12) as well as the communication DMMSE in (16). Since the CRB in (12) monotonically reduces with the increasing SNR, the optimal solutions for uniform waveform designs in (17), (18), and (19) will continuously improve with the decrease in the target distance ρ. Additionally, with decreasing ρ, the optimal number of preambles, $M_{\rm U}^*$, in (18) will decrease, $M_{\rm U}^*$ in (19) will be constant, and the change in $M_{\rm U}^*$ will be adapted based on the rate of decrease in the radar CRB with ρ for weighted average optimization-based design in (17). With an increase in K in JCR problem formulations, the CRB in (12) degrades and its existence depends on $M_{\rm U}$. Therefore, with growing K, the optimal solutions for uniform waveform designs in (17) as well as in (18) will rapidly degrade with a steep increase in $M_{\rm U}^*$, while the feasibility of optimal waveform design in (17), (18), and (19) will be severely limited. Additionally, the optimal solutions achieved by adaptive JCR waveform designs for all three problems are limited. This is because the use of multiple frames placed at the Nyquist rate in a CPI will lead to a large physical increase in the preamble duration, thereby significantly decreasing the communication spectral efficiency. These insights are further explained in Section VII.

B. Non-uniform waveform design

For non-uniform waveform designs, $M_{\rm V}$ frames are non-uniformly placed in a CPI of $T \geq M_{\rm V} T_{\rm D}$, as shown in Fig. 3(b). Therefore, the preambles are placed in a sub-Nyquist fashion with varying $N_m T_{\rm s} \geq T_{\rm D}$ spacing between them. Here, the $m^{\rm th}$ frame is located at $q_m \geq m$ and the set of all preamble locations in a CPI $\mathcal{M}_{\rm V} = \{q_m, 1 \leq m \leq M_{\rm V}\}$ is a sparse subset of the contiguous set $\mathcal{M} = \{1, 2, \cdots, T/T_{\rm D}\}$ that guarantees the desirable velocity estimation performance. The location of preambles in a CPI can be chosen randomly or in a determined fashion.

The VP locations for the non-uniform waveform is obtained using the following difference co-waveform of $\mathcal{M}_{\rm V}$

$$\mathcal{C}_{\rm V} = \{q_m - q_n,\ 0 \leq m, n \leq (M_{\rm V} - 1)\}. \tag{22}$$

Vectorizing $\mathbf{R}$ yields the co-waveform signal model expressed as

$$\mathbf{r} = \text{vec}(\mathbf{R}) = \mathbf{D}_{\rm q}\mathbf{p} + \sigma_{\rm n}^2 \mathbf{i}, \tag{23}$$

where $\mathbf{D}_{\rm q} \triangleq \mathbf{D}^{\rm c} \odot \mathbf{D}$ and $\mathbf{p} \triangleq [p_1, p_2, \cdots, p_K]$. The matrix $\mathbf{D}_{\rm q}$ also represents the steering matrix of $\mathcal{C}_{\rm V}$ [39].

For tractable analysis, we use deterministic non-uniform waveforms that can be represented in closed-form and contain no holes in their corresponding difference co-waveforms. MUSIC-like algorithms can then be applied on the full contiguous stretch of $|\mathcal{C}_{\rm V}|$ elements in the hole-free difference co-waveforms. The approach developed in this paper can also be extended to other sparse waveforms.

The CRB expression in (12) is valid under the condition that $2K \leq |\mathcal{C}_{\rm V}|$ for hole-free difference co-waveforms [40]. The cardinality of the difference co-waveform $\mathcal{C}_{\rm V}$ depends on the placements of non-uniform preambles $\mathcal{M}_{\rm V}$ and can be used to identify $\mathcal{O}(M_{\rm V}^2)$ sources. For $K << M_{\rm U}$ and $M_{\rm U} = M_{\rm V} = M$, the CRB for non-uniform waveforms also decreases much faster than for uniform waveforms as M increases [31]. At $K > M_{\rm V}$, however, the CRB for the non-uniform waveform design may not reduce to zero when SNR goes to infinity. Additionally, the CRB metric can be non-convex with respect to $M_{\rm V}$ for non-uniform waveform, as illustrated later in Section VII.

Since the non-uniform waveform design usually needs a lower $M_{\rm V}$ to achieve a given radar CRB and a much higher $M_{\rm V}$ to achieve a valid CRB for a given K than a uniform waveform design, a non-uniform waveform design allows a larger set of feasible solutions for the JCR waveform optimization problems in (17), (18), and (19). Additionally, the lower the cardinality of the sparse set $\mathcal{M}_{\rm V}$, the smaller the overhead on the effective communication spectral efficiency. Therefore, non-uniform waveform design allows a reduced trade-off between the radar CRB and the communication DMMSE for low target density, thereby resulting in an enhanced optimal JCR waveform design. The saturation effect observed in non-uniform waveform design at high SNR, however, reduces the advantage of non-uniform JCR waveform design over uniform JCR waveform design at small radar distances.

Among several redundancy waveforms with no holes [52], Wichmann and nested waveforms are relevant. The *Wichmann virtual waveform (WVW)* is known to yield the largest aperture co-waveform for all redundancy waveforms with more than 8 elements [17]. The inter-preamble spacings of the WVW is [53]

$$\begin{aligned} d\mathcal{M}_{\rm W} = \{&1^{(a_1)}, a_1+1, (2a_1+1)^{(a_2)}, (4a_1+3)^{(a_2)}, \\ &(2a_1+2)^{(a_1+1)}, 1^{(a_1)}\}, \end{aligned} \tag{24}$$

where $a_1, a_2 \in \mathbb{N}$ and the notation $a_1^{(a_2)}$ represents a_2 repetitions of a_1. The VP count $|\mathcal{C}_{\rm W}|$ of the WVW is

$$|\mathcal{C}_{\rm W}| = 4a_1(a_1+a_2+2) + 3(a_2+1). \tag{25}$$

Therefore, the weighted average formulation in (17) can be modified after incorporating the WVW structure into the problem formulation as:

$$\begin{aligned} \underset{a_1, M_{\rm W}}{\text{minimize}} \quad & \omega_{\rm r}\varphi_{\rm r}(\text{CRB}) + \omega_{\rm c}\varphi_{\rm c}(\text{DMMSE}) \\ \text{subject to} \quad & \{T, K, \rho\} = \text{constants}, \\ & 4a_1 + a_2 + 3 = M_{\rm W} \leq T/T_{\rm D}, \qquad (26) \\ & \{q_m - q_{m-1}\}_{m=1}^{M} = d\mathcal{M}_{\rm W}, \\ & a_1, a_2 \in \mathbb{N}, \qquad (27) \end{aligned}$$

where the radar CRB for the WVW exists when $2K \leq |\mathcal{C}_{\rm W}|$. The other constrained optimization formulations in (18) and in (19) can be similarly modified by incorporating the WVW structure into the formulations.

In most of the prior work in sparse array optimization, $|\mathcal{C}_{\rm v}|$ is maximized for a given $|\mathcal{M}_{\rm V}|$. Using this traditional optimization criteria, optimum a_1^* is the closest non-negative integer solution to $(|\mathcal{M}_{\rm V}| - 4)/6$ and optimum $a_2^* = |\mathcal{M}_{\rm V}| - 4a_1^* - 3$ [52]. The fraction of communication data symbols $1 - \mu_{\rm W}^*$ for the WVW in a CPI is

$$1 - \mu_{\rm W}^* = 1 - \frac{(4a_1^* + a_2^* + 3)PT_{\rm s} + M_{\rm W}^* T_{\rm IFS}}{T}, \tag{28}$$

where $M_{\rm W}^*$ is the optimal minimum $|\mathcal{M}_{\rm V}|$ for the WVW and $T_{\rm IFS}$ is the interframe spacing. In Section VII, we will compare a_1^* and a_2^* values obtained using the VP count-based optimization and the CRB-based optimization.

The *Nested virtual waveform (NVW)* is widely used in MIMO radar for direction-of-arrival estimation [39]. It is obtained by nesting two uniform waveforms with different inter-element spacing. The inter-preamble spacing in the two-level NVW is

$$d\mathcal{M}_{\rm N} = \{1^{(M_1)}, (M_1+1)^{(M_2)}\}, \tag{29}$$

where M_1 is the number of preambles in the first uniform waveform and M_2 is the number of preambles in the second uniform waveform. The VP count of the NVW is

$$|\mathcal{C}_{\rm N}| = M_2(M_1+1) - 1. \tag{30}$$

Therefore, the weighted average formulation in (17) can be modified after incorporating the NVW structure into the problem formulation is given as:

$$\begin{aligned} \underset{M_1, M_{\rm N}}{\text{minimize}} \quad & \omega_{\rm r}\varphi_{\rm r}(\text{CRB}) + \omega_{\rm c}\varphi_{\rm c}(\text{DMMSE}) \\ \text{subject to} \quad & \{T, K, \rho\} = \text{constants}, \\ & M_1 + M_2 = M_{\rm N} \leq T/T_{\rm D}, \qquad (31) \\ & \{q_m - q_{m-1}\}_{m=1}^{M_{\rm N}} = \{1^{(M_1)}, (M_1+1)^{(M_2)}\}, \\ & 0 < M_1 \leq M_2, \qquad (32) \end{aligned}$$

where the radar CRB for the NVW exists when $2K \leq |\mathcal{C}_{\rm N}|$. Similarly the other two constrained formulations in (18) and in (19) can be modified by incorporating the NVW structure into the formulations.

Based on VP count optimization, the optimal values for even $|\mathcal{M}_{\rm N}|$ is $M_1^* = M_2^* = |\mathcal{M}_{\rm N}|/2$ and for odd $|\mathcal{M}_{\rm N}|/2$ is $M_1 = M_2 + 1 = (|\mathcal{M}_{\rm N}| - 1)/2$. The fraction of communication data symbols, $1 - \mu_{\rm N}^*$, for the NVW in a CPI is

$$1 - \mu_{\rm N}^* = 1 - \frac{(M_1^* + M_2^*)PT_{\rm s} + M_{\rm N}^* T_{\rm IFS}}{T}, \tag{33}$$

where M_{N}^* is the optimal minimum $|\mathcal{M}_{\mathrm{V}}|$ for the NVW. In Section VII, we will compare M_1^* and M_2^* values obtained using the VP count-based optimization and the MMSE-based optimization.

Considering only the class of MUSIC-type algorithms for velocity estimation using non-uniform waveform design, we adopt the following velocity estimation methods: direct augmentation based MUSIC (DA-MUSIC) [54], spatial smoothing based MUSIC (SS-MUSIC) [39], and direct-MUSIC [55]. Since DA-MUSIC and SS-MUSIC share the same asymptotic first- and second- order error statistics [31] and DA-MUSIC has reduced computational complexity, this paper only focuses on DA-MUSIC. The DA-MUSIC technique is applied on the virtual preambles in the co-waveform domain, whereas direct-MUSIC is applied directly on the physical non-uniformly spaced preambles. DA-MUSIC can be applied for $K \leq M_{\mathrm{V}}$ and $K > M_{\mathrm{V}}$, whereas direct-MUSIC is applicable only for $K \leq M_{\mathrm{V}}$ under certain conditions (namely that no two sources can be separated by multiples of $2\pi/Q$ where Q is an integer which depends on the non-uniform preambles placement). Direct-MUSIC, however, is sometimes more accurate than DA-MUSIC for $K \leq M_{\mathrm{V}}$, as shown in Section VII.

VII. Simulation Results

In this section, we evaluate the performance of non-uniform virtual waveform design as compared to the uniform waveform design for different target and SNR scenarios. For illustration purposes, we consider simulation parameters based on the IEEE 802.11ad standard [24] in application to automotive scenarios [4]. In particular, we consider a carrier frequency of 60 GHz, a sampling rate of 1.76 GHz, K target velocities that are equally spaced between -45 m/s and 50 m/s, a radar cross-section of 10 dBsm, a communication receiver distance of 50 m and a radar target distance up to 100 m. We use a coherent processing interval of 1 ms with M varying between 1 and 40.

A. Performance trade-off

First, the system design trade-off between radar and communication MMSE performance metrics for different virtual waveform designs is studied for various target and SNR parameters. Then, the convex approximation of the design trade-off curve for improved JCR performance is described. Lastly, MMSE achievable by non-uniform designs are explored. In particular, sparse ($K/M << 1$) and dense ($K/M \approx 1$ or $K/M >> 1$) target scenarios as well as low and high SNR use cases are investigated.

Figs. 4(a) and 4(b) depict the trade-off between the radar CRB and the communication DMMSE metrics with respect to the number of frames, M, for uniform, nested, and Wichmann waveforms. In particular, radar target distances of 5 m, 20 m, and 100 m are considered for target count $K = 1$ in Fig. 4(a) and for $K = 30$ in Fig. 4(b). For M frames in a CPI, the optimal VP count-based nested waveform with parameters M_1^* and M_2^*, as well as Wichmann waveform with parameters a_1^* and a_2^* are considered for simplicity in Figs. 4(a) and 4(b). Fig. 4(c), however, shows the 2-D JCR objective region

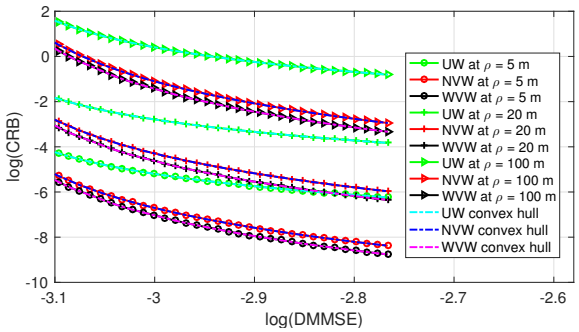

(a) Single-target with $K = 1$

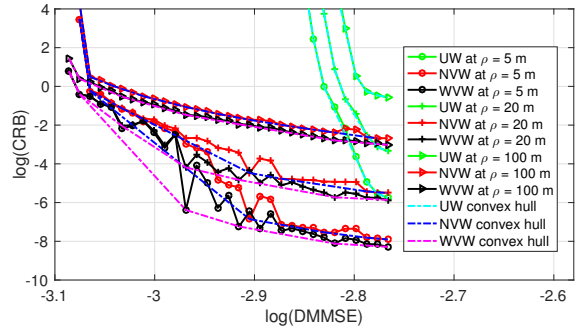

(b) Multi-target with $K = 30$

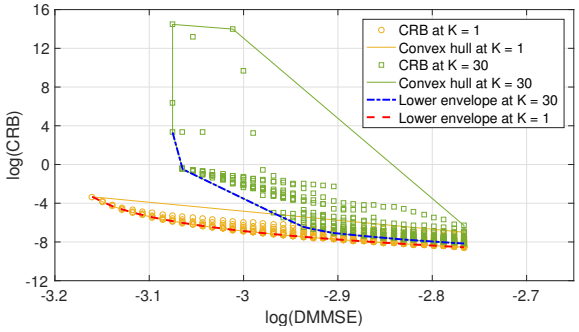

(c) Varying M and M_1 for NVW at $\rho = 5$ m.

Fig. 4. The radar CRB and the communication DMMSE pairs in the JCR trade-off region with respect to the optimization variable M along with their respective convex hulls at different target counts and distances. (a) Trade-off curves are approximately convex for small target count K for both uniform and non-uniform waveforms. (b) At large K, however, the non-convexity increases for non-uniform waveforms. (c) MMSE-based achievable 2-D JCR objective values region and its convex hull for the nested virtual waveform with varying M and different configuration parameters M_1.

achievable by nested virtual waveform for varying M as well as different configuration parameters of $1 < M_1 \leq \lfloor M/2 \rfloor$ with $M_2 = M - M_1$ at $K = 1$ and $K = 30$ for radar target distance of 5 m. The number of possible combinations of different configuration parameters $\{M_1, M_2\}$ for a given M scales almost linearly with M. Later, in Fig. 11, the CRB-based optimization is compared with the optimization based on the VP count of virtual waveforms.

Figs. 4(a) and 4(b) indicate that the radar CRB for a given communication DMMSE is the lowest in case of Wichmann virtual waveform, followed by nested virtual waveform and lastly uniform waveform. For a single target scenario in Fig. 4(a), we can see that the advantage of virtual waveforms over uniform one is more significant as the communication

DMMSE (higher M) worsens. In a multi-target scenario in Fig. 4(b), the radar CRB for uniform waveform exists only for high communication DMMSE with $M > K$, whereas the radar CRBs for virtual waveforms exist even for low communication DMMSE with $M < K$. At low communication DMMSE, we also observe that the radar CRBs achieved by virtual waveforms saturate at high SNR and large K/M ratio. In Fig. 4(c), we can see that the variation of the radar CRB with the number of targets increases at low communication DMMSE (or, small M).

Figs. 4(a) and 4(b) explore the convexity aspect of the JCR trade-off curve with respect to the number of frames M for different waveforms, whereas Fig. 4(c) illustrates the non-convexity aspect of the achievable 2-D JCR objective values region for nested waveform with varying M and configuration parameter $1 < M_1 \leq \lfloor M/2 \rfloor$. In a sparse target scenario with $K = 1$, the trade-off curves appear convex. In the case of a dense target scenario with $K = 30$, however, the trade-off curves deviate farther from convexity as the radar target distance decreases. The trade-off curve for a uniform waveform is more visibly convex than that for the non-uniform waveforms. Although the communication DMMSE is linear with respect to M (as can be seen from (15)), the achievable JCR objective values region/trade-off curve are non-convex due to the non-convexity of radar CRB with respect to M. The non-convexity of radar CRB over M is either because of the occurrence of non-decreasing CRB points with increasing M or due to the saturation effect observed for $M < K$ at small target distances.

Fig. 4(a)-(c) also illustrate the convex hull of the achievable JCR objective values region, which is the smallest convex set containing the achievable JCR objective values region and can be obtained using computational geometry algorithms [56]. In Fig. 4, we use 'convhull' function of MATLAB to obtain the convex hull. Then, we find the optimal solutions for CRB-based optimization by choosing the lower envelope of the convex hull. The use of the lower envelope of the convex hull enabled us to discard the not so beneficial trade-off points (M), such as the non-decreasing CRB points or the points in the saturation region. Additionally, the convex hull solution is achievable by using time-sharing or probabilistic occurrence techniques on the extreme points of the convex hull, similar to multi-user communication rate optimization [48]. Therefore, the convex hull approach will lead to enhanced optimal solutions for JCR waveform designs by achieving lower radar CRB for a given communication DMMSE.

We evaluate the estimation performance achieved by MUSIC-based algorithms using the mean square error (MSE) metric defined as

$$\mathrm{MSE_v} \triangleq \mathbb{E}\left[(\mathbf{v}-\hat{\mathbf{v}})(\mathbf{v}-\hat{\mathbf{v}})^*\right], \tag{34}$$

where $\mathbf{v} \triangleq [v_0, v_1, \cdots, v_{K-1}]$ is the true velocity vector and $\hat{\mathbf{v}}$ is the velocity vector estimated using the MUSIC-based algorithms. Fig. 5 compares the scalar MSE metric, $\varphi_{\mathrm{r}}(\mathrm{MSE}) \triangleq \frac{1}{K}\mathrm{Tr}\left[\log \mathrm{MSE_v}\right]$, with the corresponding scalar radar CRB metric $\varphi_{\mathrm{r}}(\mathrm{CRB}) \triangleq \frac{1}{K}\mathrm{Tr}\left[\log \mathrm{CRB}\right]$ for all three waveforms tested in a two-target scenario with $M = 20$ and varying number of snapshots and target distances. It can be seen from Fig. 5(a) that direct-MUSIC, in general, achieves CRB more efficiently than DA-MUSIC at high SNR and is very close to the CRB values even with a small number of snapshots. For the low SNR scenario in Fig. 5(b), however, DA-MUSIC performs more efficiently than direct-MUSIC and it takes fewer snapshots to approach the CRB. MUSIC-based algorithms perform closer to the CRB for low SNR in the case of the uniform waveform as compared to the virtual waveforms.

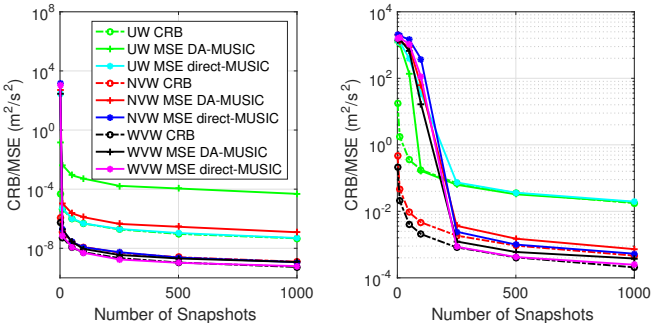

(a) $K = 2$ and $\rho = 5$ m (b) $K = 2$ and $\rho = 100$ m

Fig. 5. Comparison between MSE of MUSIC-based algorithms with the CRB for the two-target scenario at different target distances. The MUSIC-based algorithms with a small number of snapshots achieve the CRB at high SNR, while they need a higher number of snapshots at low SNR.

The MSE curves of MUSIC-based algorithms suggest that the applicability of the CRB-based optimization for joint waveform design depends on the number of available snapshots, which are limited as described in Section IV-B. The MUSIC-based algorithms are used here for illustrating the average approachability of the CRB, but of course in the case of a small number of snapshots it can be enhanced by using other algorithms, such as greedy single-snapshot grid-based algorithms [57] and nuclear norm minimization [58], or by exploiting waveforms with holes in their difference co-waveforms, such as Golomb and coprime waveforms. This is, however, out-of-scope of this paper and is left for future work.

B. Optimal waveform designs

In this subsection, we investigate the optimal solutions for three MMSE-based waveform design formulations proposed in Section V. We also compare our MMSE-based waveform optimization formulation with the more traditional VP count-based formulation.

1) Weighted average optimization-based design: In this example, we explore the optimal communication DMMSE and radar CRB via weighted average problem formulation (17). First, we study the effect of weighting on the optimal solutions, followed by the effect of target count and SNR on the optimal solutions for all three tested waveforms.

Figs. 6(a) and 6(b) show the optimal number of frames M for uniform and nested waveforms with different normalized communication weightings $0.5 \leq \omega_{\mathrm{c}} \leq 1$ at target counts $K = \{1, 10, 30\}$ for target distance $\rho = 5$ m, as well as at target distances $\rho = \{5, 100\}$ meters for $K = 10$. Additionally, the radar CRB is first normalized by a factor of 0.5 to achieve value comparable to the communication DMMSE, and then

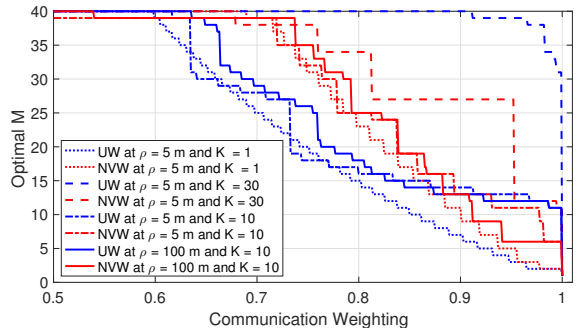

(a) Optimal M

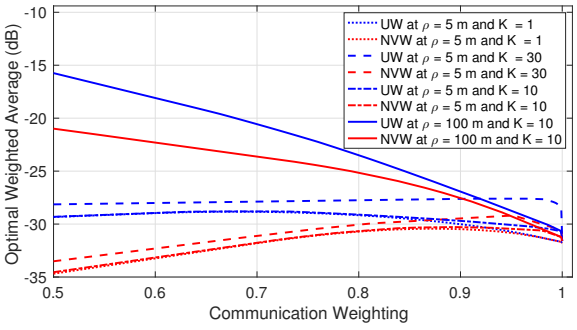

(b) Optimal weighted average

Fig. 6. Optimal number of frames M and weighted average for uniform and nested waveforms with different normalized communication weightings. (a) The optimal M decreases with varying step-size as the communication weighting increases. (b) The advantage of the nested waveform over the uniform one decreases as the communication weighting approaches 1.

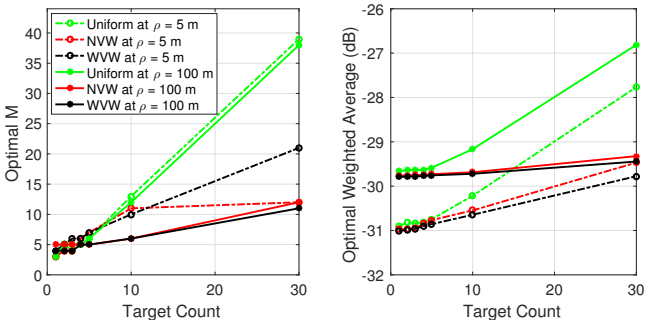

(a) Variation with K (b) Variation with K

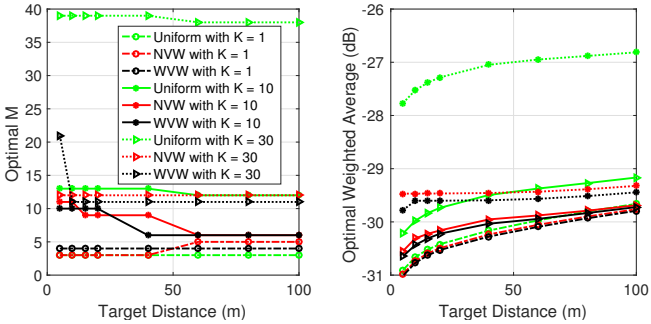

(c) Variation with ρ (d) Variation with ρ

Fig. 7. Optimal M and corresponding weighted average JCR MMSE with communication weighting of 0.96. The legend in (a) and (b) is the same, as well as in (c) and (d) is the same. The advantage of non-uniform waveform over uniform one increases with the target count, whereas it reduces with radar SNR at high target count due to the saturation effect.

further scaled with normalized radar weighting $0.5 \leq 2\omega_{\rm r} \leq 1$ to obtain the optimal solutions for weighted average optimization. The optimal M for different waveforms decreases from highest possible $M = 40$ used in a CPI for $\omega_{\rm c} = 0.5$ to the lowest feasible $M = 1$ for $\omega_{\rm c} = 1$. In simulations for Fig. 6, we use an upper limit on M because using a very high M would increase the computational complexity and might not be supported by the communication protocol. Additionally the upper limit on M is chosen to sufficiently meet the requirement of the application scenario – automotive, in our case, with velocity accuracy requirement of -10 dB [59]. At $\omega_{\rm c} = 1$, the optimal JCR waveform will be a pure communication waveform with a DMMSE of -3.2 dB. The optimal JCR performance at $\omega_{\rm c} = 0$, however, will be a pure radar performance with CRB of -86 dB at a radar target distance of 5 m and of -34 dB at a radar target distance of 100 m.

In Fig. 6(a), the optimal M varies significantly with K because of the CRB existence and the saturation effect observed at high SNR and high K/M ratio. The rate of decrease in the optimal M with respect to the communication weighting for a sparse target scenario is larger for non-uniform waveforms as compared to uniform waveform because a higher rate of decrease in the radar CRB is achieved by non-uniform waveforms with an increase in the communication DMMSE. The step size of the decrease in the optimal M with increasing communication weighting for a dense target scenario at high radar SNR is generally small for uniform waveform as compared to non-uniform waveforms due to the approximate convexity of the weighted average JCR performance metric for the uniform waveform. The step-size also depends on the presence of non-decreasing radar CRB points with increasing communication DMMSE in the corresponding trade-off curve.

Fig. 6(b) shows the optimal weighted average of the communication DMMSE and the radar CRB for different normalized communication weightings $0.5 \leq \omega_{\rm c} \leq 1$ at $K = 1$, 10, and 30 for $\rho = 5$ m, as well as at $\rho = 5$ m and 100 m for $K = 10$. The advantage of the nested waveform over uniform for a given K and ρ decreases as communication weight $\omega_{\rm c}$ approaches 1. The performance of all waveforms tested converge exactly for $\omega_{\rm c} \to 1$ at $K = 1$, because the lowest possible M is used in this case. At $\omega_{\rm c} \to 1$, the gap between the optimal performance of uniform and non-uniform waveforms increases with K due to higher M needed for the CRB to exist, while it remains constant with ρ at $K = 10$. At $\omega_{\rm c} = 1$, the JCR waveform converges to a pure communication waveform. For most of the scenarios, nested waveform performs the best and uniform one performs the worst. The insights derived for nested waveform similarly can be extended for Wichmann waveform, and Wichmann waveform generally performs better than nested as can be seen in Figs. 7(a)-(d).

Figs. 7(a) and 7(b) show the variation of optimal M and corresponding weighted average JCR MMSE-based metrics with K for communication weighting of 0.96. The optimal M increases with target count in most of the cases, except for the nested waveform at high SNR and large K that suffers

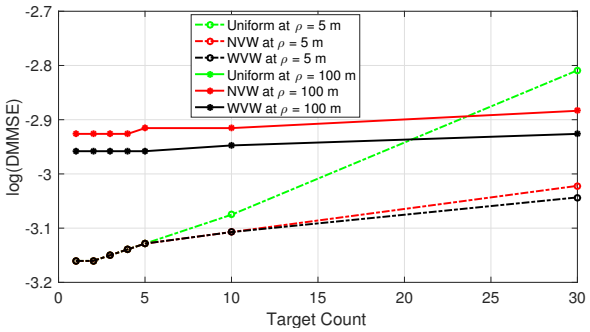

(a) Variation with target count

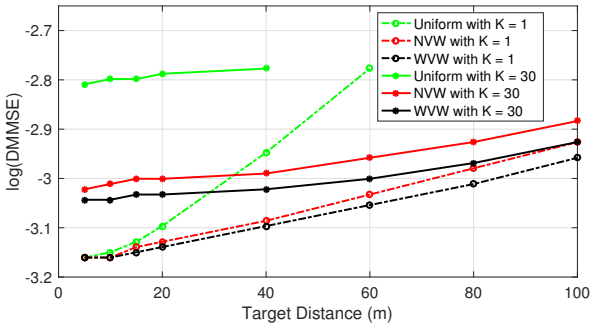

(b) Variation with target distance

Fig. 8. Optimal communication DMMSE (and corresponding optimal M) for a given minimum radar CRB constraint $\Upsilon_{\mathrm{r}} = 1.5$ cm^2/s^2. The advantage of virtual waveforms over uniform one increases with target count at small target distance and also with distance at low target count.

from saturation effect. The choice of optimal M in the case of Wichmann waveform as compared to uniform one increases with target count, and the optimal M for all three waveforms tested converges to the same value at low target count. The optimal weighted average for uniform waveform is the worst (largest) in all the cases. The optimal weighted average degrades with increasing target count, and the advantage of non-uniform waveform over uniform one increases with K, whereas it reduces with radar SNR at high K due to the saturation effect.

Figs. 7(c) and 7(d) depict the variation of optimal M and corresponding weighted average JCR MMSE-based metrics with ρ for communication weighting of 0.96. Fig. 7(c) shows that the optimal M increases with distance at low target count and decreases with distance at high target count. This effect is due to the radar CRB degradation that happens because of pathloss increasing at large distances for low target count and saturation effect increasing at small distances for high target count. Fig. 7(d) demonstrates that the optimal weighted average for uniform waveform is the worst in all the cases. The optimal weighted average for all three waveforms tested generally improves with decreasing distance. For $K = 30$, however, the saturation effect can be seen for nested and Wichmann waveforms. The rate of improvement in optimal weighted average with increasing radar SNR reduces with growing K for non-uniform waveforms, whereas it remains constant for uniform waveform.

2) Radar CRB constrained optimization-based design: In this example, we investigate optimal communication DMMSE

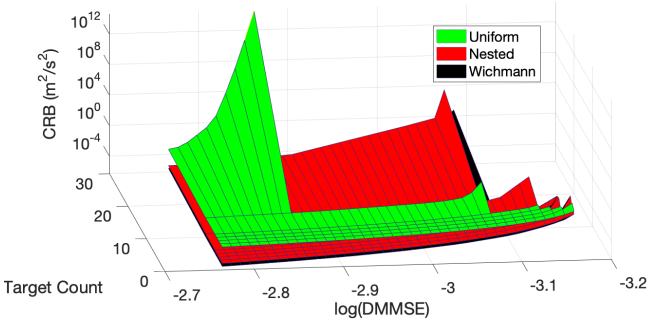

Variation with K and DMMSE for $\rho = 20$ m.

Fig. 9. The mesh plot of the optimal radar CRB for various minimum communication DMMSE constraints at different K scenarios for a radar target distance of 20 m. The gap between the performances of all the three tested waveforms improve with increasing target count and communication DMMSE.

(and corresponding optimal M) for a given minimum radar CRB constrained problem formulation (18) in different target density and SNR scenarios. Fig. 8 shows the optimal DMMSE solution for a minimum radar CRB of -18 dB. Wichmann waveform performs the best, followed by nested waveform. The advantage of virtual waveforms over uniform one increases with target count at high SNR and also with distance at low target density. Performances of all three waveforms tested (Wichmann, nested, and uniform) converge at low target count and small target distance. The optimal communication DMMSE increases with growing target count and decreasing radar SNR. Optimal communication DMMSE, however, is less effected by target count at small distances, as compared to the large distances. Additionally, the rate of increase of optimal communication DMMSE with increasing target distance is faster at lower K. These effects can be explained using the saturation effect at high K/M ratio and high SNR. The effect of the preamble count can also be seen on the feasibility of uniform solutions. The insights for optimal M are similar due to its linear relation with communication DMMSE.

3) Communication DMMSE constrained optimization-based design: In this example, we examine the optimal radar CRB achieved by all three waveforms tested for a given minimum communication DMMSE constrained problem formulation (19). First, we study the effect of different DMMSE constraints and target count on the optimal radar CRB at a given target distance. Then, we explore the effect of varying target count and distance on the optimal radar CRB for a given DMMSE constraint.

Fig. 9 depicts the lower envelope of the optimal radar CRB convex hull with respect to the target count K and communication DMMSE constraint Υ_{c} at a radar target distance $\rho = 20$ m, where the convex hull of the JCR trade-off region is obtained similar to Fig. 4. The existence of the optimal radar CRB solution depends on the target count. For $2K \leq |\mathcal{C}_{\mathrm{V}}|$, where $|\mathcal{C}_{\mathrm{V}}|$ is the VP count of the given waveform design, the optimal M that minimizes the radar CRB for a given communication DMMSE may exist and it corresponds to the maximum M that satisfies the communication DMMSE bound Υ_{c} on the convex hull of the JCR trade-off curve for a given CPI. Therefore, the existence of optimal radar

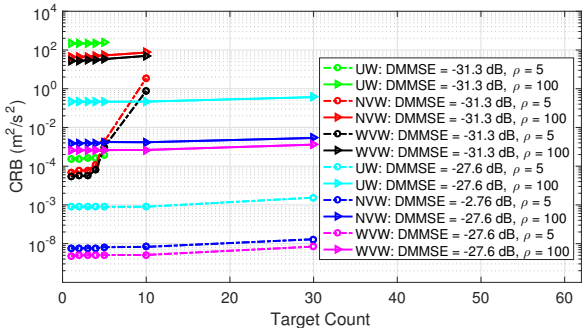

(a) Variation with K for $\rho = \{5, 100\}$ m.

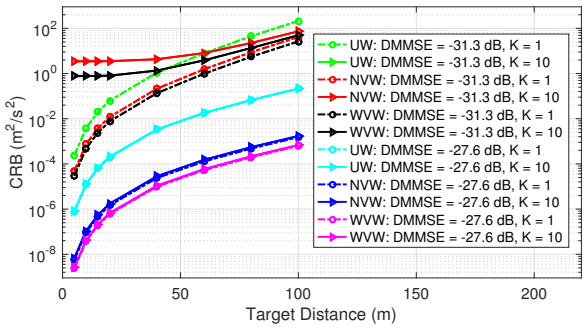

(b) Variation with ρ for $K = \{1, 10\}$.

Fig. 10. Optimal radar CRB for a communication DMMSE of -31.3 dB and -27.6 dB. The advantage of virtual waveforms over the uniform one is more than 10 dB at high communication DMMSE.

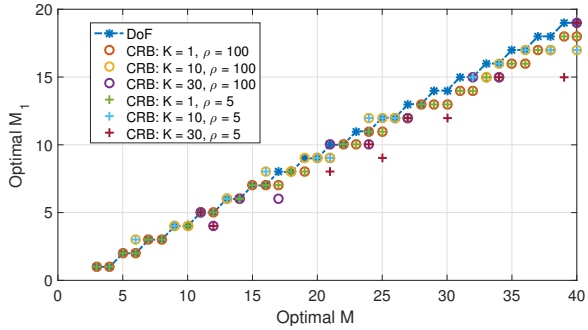

(a) Optimal configuration parameter M_1

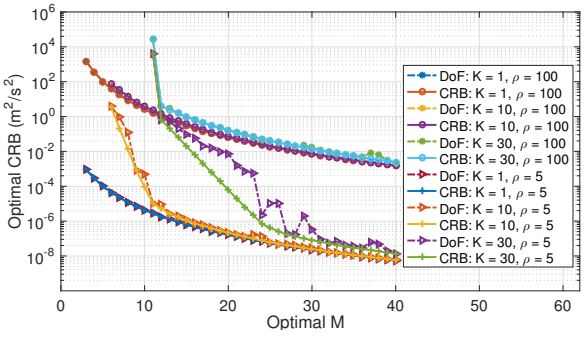

(b) Optimal radar CRB

Fig. 11. Comparison between the VP count-based optimization and the CRB-based optimization for nested waveform. The gap between the optimal solutions of both the optimizations grows with increasing target count and decreasing target distance.

CRB solution for a given communication DMMSE and K is the least restricted for the Wichmann waveform, whereas it is the most restricted for the uniform one. Additionally, the optimal CRB obtained for the Wichmann waveform is better than the nested one, followed by the uniform one. The gaps between the optimal radar CRB values found for all the three tested waveforms improve with increasing target count and communication DMMSE. Additionally, the optimal radar CRBs for all three waveforms tested converge at low communication DMMSE.

Fig. 10 shows the optimal radar CRB for all three waveforms tested with communication DMMSE bounds $\Upsilon_c = -31.3$ dB and $\Upsilon_c = -27.6$ dB at target counts $K = 1$ and $K = 30$ and radar target distances $\rho = 5$ m and 100 m. The solutions to the DMMSE-constrained formulation in (19) simplifies to finding the maximum number of frames M that meets the required DMMSE constraint using (15), and then to finding the optimal radar CRB corresponding to the obtained optimal M on the convex hull of the JCR trade-off curve. For DMMSE of -31.3 dB, the optimal M is 6, while for DMMSE of -27.6 dB, the optimal M is 40 for all those scenarios where the radar CRB solution exists.

For all three waveforms tested, Fig. 10(a) depicts that the optimal radar CRB degrades with increasing target count and Fig. 10(b) shows the optimal radar CRB grows with increasing radar distance. In most cases, the Wichmann waveform performs the best and uniform one performs the worst. At high communication DMMSE with the optimal $M = 40$, the Wichmann waveform achieved more than 10 dB improvement in the velocity estimation CRB as compared to the uniform one. Fig. 10(a) shows that the performances of all three waveforms tested converge at low communication DMMSE and high SNR (ρ = 5 m) with high target density K/M (K = 5 and M = 6), if the CRB exist for all three tested waveforms. Fig. 10(b) shows the saturation effect at high SNR (small ρ) with high K/M ($K = 10$ and $M = 6$) ratio for nested and Wichmann waveforms, while the uniform waveform is not feasible due to $K \geq M$. The radar CRB achieved for virtual waveforms at low communication DMMSE with the optimal $M = 6$ is effected by the change in target count K for small target distances, whereas the optimal radar CRB is only slightly effected at long distances. At high communication DMMSE, however, this saturation effect is not observed.

4) Comparison with VP count optimization-based design: Fig. 11(a) and Fig. 11(b) explore the optimal configuration parameter M_1 and radar CRB that maximizes the VP count (or, equivalently degrees of freedom (DoF)) using nested waveform for a given M. The figures also compare the virtual preamble count-based optimization with its respective CRB-based communication DMMSE constrained optimization-based design, which was formulated in (18) and illustrated in the previous subsection, for different K and radar SNR. For odd M, the unique optimal M_1 solution using the VP count-based optimization is $(M-1)/2$ and for even M there are two solutions $M/2$ and $M - 1/2$. Fig. 11 uses the smallest optimal M_1 as VP count optimization-based one and we see that this optimal M_1 increases step-wise linearly with M.

For $K = 1$, the optimal M_1 for both the optimizations

match at small M and start deviating a little for higher M. Fig. 11(a) demonstrates that for $K = 1$, the radar CRB for both problem formulations are very close to each other at high SNR. The solutions, however, start to deviate for high target count and high radar SNR. Similar insights can be drawn for Wichmann waveform with configuration parameters a_1 and q, but this study is excluded from the paper due to space constraint. Fig. 11 suggests that the VP count optimization-based design can be used as a coarse estimate for the CRB-based communication DMMSE constrained solution.

VIII. Conclusion and discussion

In this paper, we proposed an adaptive virtual waveform design for a millimeter-wave joint communication-radar system that enjoys the benefit of a fully-digital baseband processing in the time-domain and a high available bandwidth. Our proposed waveform exploits only a few non-uniform preambles in a CPI and sparse sensing techniques to achieve high velocity estimation accuracy without reducing communication data rate much. We developed a novel communication DMMSE metric to accurately quantify the trade-off with radar CRB for a JCR waveform design.

The performance trade-off curve between the radar CRB and communication DMMSE contained some non-convex points due to the occurrence of non-decreasing CRB points with increasing communication DMMSE or due to the radar CRB saturation at high SNR. To improve the optimal JCR performance, we discarded these undesirable non-convex points by using a convex hull approximation of the trade-off curve. Then, we formulated three different MMSE-based problems to optimize the trade-off between communication and radar: a minimum communication DMMSE constrained formulation, a minimum radar CRB constrained formulation, as well as a weighted MMSE average formulation. To reduce the computation complexity for finding optimal waveform solutions, we used specific waveform configurations – the uniform waveform, the nested virtual waveform, and the Wichmann virtual waveform. Numerical results demonstrated that, in most cases, non-uniform waveforms perform much better than uniform waveforms, especially at low SNR and high target density. Additionally, we observed that the traditional virtual preamble count-based solution can be used as a coarse estimate of the optimal solution for our MMSE-based optimization problems.

The results in this paper can be taken into account to design an adaptive virtual waveform that achieves simultaneous high communication data rate and super-resolution radar estimation for next-generation mmWave devices. For future work, the proposed framework can be extended to other virtual waveforms, such as the Golomb waveform and the coprime waveform. The achievability of their CRBs can be investigated using more advanced estimation algorithms, such as nuclear norm minimization. This may lead to better performance at a low number of snapshots. This work can also be extended for a more general Ricean fading mmWave channel model with a small number of scattering clusters. It would be interesting to see how the Ricean fading factor and the additional block sparse structure will impact the advantage of the virtual waveforms that exploit compressive sensing techniques on the channel covariance matrix.

Additionally, the work in this paper can be extended to investigate the effect of relative spacing between target velocities on the MMSE-based virtual JCR waveform design. When the target velocities are well-spaced beyond the minimum resolution of the virtual waveform, the CRB metric is not dependent on the relative spacing as illustrated in [55]. This can be realized using low communication weighting in the weighted average optimization-based design, using low radar CRB in the radar CRB constrained optimization-based design, and using high communication DMMSE constraint in the communication DMMSE constrained optimization-based design, which will allow only those feasible values of optimal M that achieve accuracy higher than the minimum velocity resolution. The DMMSE will not be effected by the target spacing either because the two-way multi-target radar channel and the one-way frequency-selective communication channel are assumed to be independent in our paper. In future work, the effect on DMMSE can be analyzed either by incorporating stochastic geometry or by real experiments. Currently, there is no known real automotive data available for wide-band JCR at the mmWave band as per our knowledge that can be used to proceed in this line of research.

References

[1] P. Kumari, D. H. N. Nguyen, and R. W. Heath, "Performance trade-off in an adaptive IEEE 802.11ad waveform design for a joint automotive radar and communication system," in *Proc. IEEE Int. Conf. Acoust., Speech and Signal Process.*, March 2017, pp. 4281–4285.

[2] P. Kumari, S. A. Vorobyov, and R. W. Heath, "Virtual pulse design for IEEE 802.11ad-based joint communication-radar," in *Proc. IEEE Int. Conf. Acoust., Speech and Signal Process.*, April 2018, pp. 3315–3319.

[3] J. Choi, V. Va, N. Gonzalez-Prelcic, R. Daniels, C. R. Bhat, and R. W. Heath, "Millimeter-wave vehicular communication to support massive automotive sensing," *IEEE Commun. Mag.*, vol. 54, no. 12, pp. 160–167, December 2016.

[4] S. M. Patole, M. Torlak, D. Wang, and M. Ali, "Automotive radars: A review of signal processing techniques," *IEEE Signal Processing Mag.*, vol. 34, no. 2, pp. 22–35, March 2017.

[5] M. Kunert, "The EU project MOSARIM: A general overview of project objectives and conducted work," in *Proc. European Radar Conf.*, Oct 2012, pp. 1–5.

[6] A. Bourdoux, U. Ahmad, D. Guermandi, S. Brebels, A. Dewilde, and W. Van Thillo, "PMCW waveform and MIMO technique for a 79 GHz CMOS automotive radar," in *Proc. IEEE Radar Conf.*, May 2016, pp. 1–5.

[7] K. V. Mishra, M. R. Bhavani Shankar, V. Koivunen, B. Ottersten, and S. A. Vorobyov, "Toward millimeter-wave joint radar communications: A signal processing perspective," *IEEE Signal Processing Magazine*, vol. 36, no. 5, pp. 100–114, Sep. 2019.

[8] M. Bocquet, C. Loyez, C. Lethien, N. Deparis, M. Heddebaut, A. Rivenq, and N. Rolland, "A multifunctional 60-GHz system for automotive applications with communication and positioning abilities based on time reversal," in *Proc. European Radar Conf.*, Sep. 2010, pp. 61–64.

[9] S. H. Dokhanchi, M. R. B. Shankar, T. Stifter, and B. Ottersten, "Multicarrier phase modulated continuous waveform for automotive joint radar-communication system," in *Proc. Int. Workshop on Signal Process. Advances in Wireless Commun. (SPAWC)*, June 2018, pp. 1–5.

[10] P. McCormick, C. Sahin, S. Blunt, and J. G. Metcalf, "FMCW implementation of phase-attached radar-communications (PARC)," in *Proc. IEEE Radar Conf.*, April 2019, pp. 1–6.

[11] A. Hassanien, M. G. Amin, Y. D. Zhang, and F. Ahmad, "Signaling strategies for dual-function radar communications: an overview," *IEEE Aerospace and Electronic Systems Mag.*, vol. 31, no. 10, pp. 36–45, Oct 2016.

[12] P. Kumari, N. Gonzalez-Prelcic, and R. W. Heath Jr, "Investigating the IEEE 802.11ad Standard for Millimeter Wave Automotive Radar," in *Proc. IEEE Veh. Technol. Conf.*, September 2015, pp. 3587–3591.

[13] E. Grossi, M. Lops, L. Venturino, and A. Zappone, "Opportunistic radar in IEEE 802.11ad networks," *IEEE Trans. Signal Process.*, vol. 66, no. 9, pp. 2441–2454, May 2018.

[14] P. Kumari, J. Choi, N. González-Prelcic, and R. W. Heath, "IEEE 802.11ad-based radar: An approach to joint vehicular communication-radar system," *IEEE Trans. Veh. Technol.*, vol. 67, no. 4, pp. 3012–3027, April 2018.

[15] G. R. Muns, K. V. Mishra, C. B. Guerra, Y. C. Eldar, and K. R. Chowdhury, "Beam alignment and tracking for autonomous vehicular communication using IEEE 802.11ad-based radar," *arXiv preprint arXiv:1712.02453*, 2017.

[16] S. H. Dokhanchi, B. S. Mysore, K. V. Mishra, and B. Ottersten, "A mmWave automotive joint radar-communications system," *IEEE Trans. on Aerospace and Electronic Systems*, pp. 1–1, 2019.

[17] D. A. Linebarger, I. H. Sudborough, and I. G. Tollis, "Difference bases and sparse sensor arrays," *IEEE Trans. on Information Theory*, vol. 39, no. 2, pp. 716–721, March 1993.

[18] M. I. Skolnik, Ed., *Radar Handbook*, 2nd ed. McGraw Hill, 1990.

[19] P. P. Vaidyanathan and P. Pal, "Sparse sensing with co-prime samplers and arrays," *IEEE Trans. Signal Process.*, vol. 59, no. 2, pp. 573–586, Feb 2011.

[20] K. V. Mishra and Y. C. Eldar, "Sub-Nyquist channel estimation over IEEE 802.11ad link," in *Proc. Int. Conf. on Sampling Theory and Applications (SampTA)*, July 2017, pp. 355–359.

[21] H. Rohling and M.-M. Meinecke, "Waveform design principles for automotive radar systems," in *Proc. CIE Int. Conf. on Radar*, Oct 2001, pp. 1–4.

[22] N. A. Estep, D. L. Sounas, J. Soric, and A. Alù, "Magnetic-free non-reciprocity and isolation based on parametrically modulated coupled-resonator loops," *Nature Physics*, vol. 10, no. 12, pp. 923–927, 2014.

[23] L. Li, K. Josiam, and R. Taori, "Feasibility study on full-duplex wireless millimeter-wave systems," in *Proc. IEEE Int. Conf. Acoust., Speech and Signal Process.*, May 2014, pp. 2769–2773.

[24] "Wireless LAN Medium Access Control (MAC) and Physical Layer (PHY) Specifications. Amendment 3: Enhancements for Very High Throughput in the 60 GHz Band," *IEEE Std. 802.11ad*, 2012.

[25] P. Kumari, K. U. Mazher, A. Mezghani, and R. W. Heath, "Low resolution sampling for joint millimeter-wave MIMO communication-radar," in *Proc. IEEE Statistical Signal Processing Workshop (SSP)*, June 2018, pp. 193–197.

[26] T. S. Rappaport, G. R. MacCartney, M. K. Samimi, and S. Sun, "Wideband millimeter-wave propagation measurements and channel models for future wireless communication system design," *IEEE Trans. on Communications*, vol. 63, no. 9, pp. 3029–3056, Sept 2015.

[27] A. Bazzi, C. Kärnfelt, A. Peden, T. Chonavel, P. Galaup, and F. Bodereau, "Estimation techniques and simulation platforms for 77 GHz FMCW ACC radars," *The European Physical Journal Applied Physics*, vol. 57, no. 01, p. 11001, 2012.

[28] L. Dai, B. Wang, Y. Yuan, S. Han, C. I, and Z. Wang, "Non-orthogonal multiple access for 5G: solutions, challenges, opportunities, and future research trends," *IEEE Communications Mag.*, vol. 53, no. 9, pp. 74–81, Sep. 2015.

[29] P. Stoica and R. L. Moses, *Spectral analysis of signals*. Upper Saddle River, NJ: Prentice-Hall, 2005.

[30] Z. Yang, J. Li, P. Stoica, and L. Xie, "Sparse methods for direction-of-arrival estimation," in *Academic Press Library in Signal Processing, Volume 7*, R. Chellappa and S. Theodoridis, Eds., 2018, pp. 509–581.

[31] M. Wang and A. Nehorai, "Coarrays, MUSIC, and the Cramer-Rao bound," *IEEE Trans. Signal Process.*, vol. 65, no. 4, pp. 933–946, Feb 2017.

[32] R. W. Heath Jr and A. Lozano, *Foundations of MIMO Communication*. Cambridge University Press, 2019.

[33] K. Takizawa, M. Kyrö, K. Haneda, H. Hagiwara, and P. Vainikainen, "Performance evaluation of 60 GHz radio systems in hospital environments," in *Proc. of the IEEE Int. Conf. on Communications (ICC)*, June 2012, pp. 3219–3295.

[34] W.-C. Liu, F.-C. Yeh, T.-C. Wei, C.-D. Chan, and S.-J. Jou, "A Digital Golay-MPIC Time Domain Equalizer for SC/OFDM Dual-Modes at 60 GHz Band," *IEEE Trans. on Circuits and Systems I: Regular Papers*, vol. 60, no. 10, pp. 2730–2739, 2013.

[35] H. L. Van Trees, *Detection, estimation, and modulation theory*. John Wiley & Sons, 2004.

[36] S. M. Kay, *Fundamentals of statistical signal processing*. Prentice Hall PTR, 1993.

[37] C. L. Liu and P. P. Vaidyanathan, "New Cramer-Rao bound expressions for coprime and other sparse arrays," in *Proc. IEEE Sensor Array and Multichannel Signal Process. Workshop (SAM)*, July 2016, pp. 1–5.

[38] J. Li, L. Xu, P. Stoica, K. W. Forsythe, and D. W. Bliss, "Range compression and waveform optimization for MIMO radar: A cramer-rao bound based study," *IEEE Trans. Signal Process.*, vol. 56, no. 1, pp. 218–232, Jan 2008.

[39] P. Pal and P. P. Vaidyanathan, "Nested arrays: A novel approach to array processing with enhanced degrees of freedom," *IEEE Trans. Signal Process.*, vol. 58, no. 8, pp. 4167–4181, Aug 2010.

[40] A. Koochakzadeh and P. Pal, "Cramer-Rao bounds for underdetermined source localization," *IEEE Signal Processing Lett.*, vol. 23, no. 7, pp. 919–923, July 2016.

[41] P. Stoica and T. L. Marzetta, "Parameter estimation problems with singular information matrices," *IEEE Trans. Signal Process.*, vol. 49, no. 1, pp. 87–90, Jan 2001.

[42] I. G. Cumming and F. H. Wong, "Digital processing of synthetic aperture radar data," *Artech house*, vol. 1, no. 3, 2005.

[43] D. W. Bliss, "Cooperative radar and communications signaling: The estimation and information theory odd couple," in *Proc. IEEE Radar Conf.*, May 2014, pp. 50–55.

[44] A. Herschfelt and D. W. Bliss, "Spectrum management and advanced receiver techniques (SMART): Joint radar-communications network performance," in *Proc. IEEE Radar Conf.*, April 2018, pp. 1078–1083.

[45] B. Paul and D. W. Bliss, "Extending joint radar-communications bounds for FMCW radar with Doppler estimation," in *Proc. IEEE Radar Conf.*, 2015, pp. 89–94.

[46] T. M. Cover and J. A. Thomas, *Elements of information theory*. John Wiley & Sons, 2012.

[47] D. P. Palomar and S. Verdu, "Gradient of mutual information in linear vector Gaussian channels," *IEEE Trans. on Information Theory*, vol. 52, no. 1, pp. 141–154, Jan 2006.

[48] J. Brehmer, *Utility Maximization in Nonconvex Wireless Systems*. Springer Science & Business Media, 2012, vol. 5.

[49] S. Boyd and L. Vandenberghe, *Convex optimization*. Cambridge University Press, 2004.

[50] P. Stoica and A. Nehorai, "Performance study of conditional and unconditional direction-of-arrival estimation," *IEEE Trans. on Acoustics, Speech, and Signal Process.*, vol. 38, no. 10, pp. 1783–1795, Oct 1990.

[51] ——, "MUSIC, maximum likelihood, and Cramer-Rao bound," *IEEE Trans. on Acoustics, Speech, and Signal Process.*, vol. 37, no. 5, pp. 720–741, May 1989.

[52] R. Rajamäki and V. Koivunen, "Comparison of sparse sensor array configurations with constrained aperture for passive sensing," in *Proc. IEEE Radar Conf. (RadarConf)*, May 2017, pp. 0797–0802.

[53] B. Wichmann, "A note on restricted difference bases," *Journal of the London Mathematical Society*, vol. 1, no. 1, pp. 465–466, 1963.

[54] C. L. Liu and P. P. Vaidyanathan, "Remarks on the spatial smoothing step in coarray music," *IEEE Signal Processing Lett.*, vol. 22, no. 9, pp. 1438–1442, Sept 2015.

[55] P. P. Vaidyanathan and P. Pal, "Direct-MUSIC on sparse arrays," in *Proc. Int. Conf. on Signal Processing and Communications (SPCOM)*, July 2012, pp. 1–5.

[56] F. P. Preparata and M. I. Shamos, *Computational geometry: an introduction*. Springer Science & Business Media, 2012.

[57] Y. D. Zhang, M. G. Amin, and B. Himed, "Sparsity-based DOA estimation using co-prime arrays," in *Proc. IEEE Int. Conference on Acoustics, Speech and Signal Process.* IEEE, 2013, pp. 3967–3971.

[58] Z. Yang, J. Li, P. Stoica, and L. Xie, "Sparse methods for direction-of-arrival estimation," in *Academic Press Library in Signal Processing, Volume 7*. Elsevier, 2018, pp. 509–581.

[59] J. Hasch, E. Topak, R. Schnabel, T. Zwick, R. Weigel, and C. Waldschmidt, "Millimeter-wave technology for automotive radar sensors in the 77 GHz frequency band," *IEEE Trans. on Microwave Theory and Techniques*, vol. 60, no. 3, pp. 845–860, 2012.

Preeti Kumari received the B.Tech. degree in electronics and telecommunication engineering from Shri Guru Gobind Singhji Institute of Engineering and Technology, India, in 2009. She received the M.S. degree in electrical and computer engineering from The University of Texas at Austin, USA, in 2016, where she is currently pursuing the Ph.D. degree with the Wireless Networking and Communications Group. From 2009 to 2013, she was a Scientist with the Indian Space Research Organization (ISRO), Ahmedabad, GJ, India. She held internship positions with National Instruments, Austin, TX, USA, in 2015, Intel Corporation, Hillsboro, OR, USA, in 2016, and Qualcomm at San Diego, CA, USA, in 2018. Her research interests include radar system design, wireless communication theory, signal processing, estimation theory, and software-defined radio prototypes.

Sergiy A. Vorobyov Sergiy A. Vorobyov (M'02–SM'05–F'18) received the M.Sc. and Ph.D. degrees in systems and control from Kharkiv National University of Radio Electronics, Ukraine, in 1994 and 1997, respectively. He is a Professor with the Department of Signal Processing and Acoustics, Aalto University, Finland. He has been previously with the University of Alberta, Alberta, Canada as an Assistant, Associate and then Full Professor. Since his graduation, he also held various research and faculty positions at Kharkiv National University of Radio Electronics, Ukraine; the Institute of Physical and Chemical Research (RIKEN), Japan; McMaster University, Canada; Duisburg-Essen University and Darmstadt University of Technology, Germany; and the Joint Research Institute between Heriot-Watt University and Edinburgh University, U.K. His research interests include optimization and multi-liner algebra methods in signal processing; statistical and array signal processing; sparse signal processing; estimation and detection theory; sampling theory; and multi-antenna, very large, cooperative, and cognitive systems.

Dr. Vorobyov is a recipient of the 2004 IEEE Signal Processing Society Best Paper Award, the 2007 Alberta Ingenuity New Faculty Award, the 2011 Carl Zeiss Award (Germany), the 2012 NSERC Discovery Accelerator Award, and other awards. He is serving as Senior Area Editor for IEEE SIGNAL PROCESSING LETTERS since 2016. He served as an Associate Editor for the IEEE TRANSACTIONS ON SIGNAL PROCESSING in 2006–2010 and the IEEE SIGNAL PROCESSING LETTERS in 2007–2009. He was a member of the Sensor Array and Multi-Channel Signal Processing and Signal Processing for Communications and Networking Technical Committees of the IEEE Signal Processing Society in 2007–2012 and 2010–2016, respectively. He has served as the Track Chair for Asilomar 2011, Pacific Grove, CA; the Technical Co-Chair for IEEE CAMSAP 2011, Puerto Rico; the Tutorial Chair for ISWCS 2013, Ilmenau, Germany; and the Technical Co-Chair for IEEE SAM 2018, Sheffield, U.K.

Robert W. Heath Jr. (S'96 - M'01 - SM'06 - F'11) received the B.S. and M.S. degrees from the University of Virginia, Charlottesville, VA, in 1996 and 1997 respectively, and the Ph.D. from Stanford University, Stanford, CA, in 2002, all in electrical engineering. From 1998 to 2001, he was a Senior Member of the Technical Staff then a Senior Consultant at Iospan Wireless Inc, San Jose, CA where he worked on the design and implementation of the physical and link layers of the first commercial MIMO-OFDM communication system. Since January 2002, he has been with the Department of Electrical and Computer Engineering at The University of Texas at Austin where he is a Cullen Trust for Higher Education Endowed Professor, and is a Member of the Wireless Networking and Communications Group. He is also President and CEO of MIMO Wireless Inc. He authored "Introduction to Wireless Digital Communication" (Prentice Hall, 2017) and "Digital Wireless Communication: Physical Layer Exploration Lab Using the NI USRP" (National Technology and Science Press, 2012), and co-authored "Millimeter Wave Wireless Communications" (Prentice Hall, 2014).

Dr. Heath has been a co-author of sixteen award winning conference and journal papers including the 2010 and 2013 EURASIP Journal on Wireless Communications and Networking best paper awards, the 2012 Signal Processing Magazine best paper award, a 2013 Signal Processing Society best paper award, 2014 EURASIP Journal on Advances in Signal Processing best paper award, the 2014 Journal of Communications and Networks best paper award, the 2016 IEEE Communications Society Fred W. Ellersick Prize, the 2016 IEEE Communications and Information Theory Societies Joint Paper Award, and the 2017 Marconi Prize Paper Award. He received the 2017 EURASIP Technical Achievement award. He was a distinguished lecturer in the IEEE Signal Processing Society and is an ISI Highly Cited Researcher. He is also an elected member of the Board of Governors for the IEEE Signal Processing Society, a licensed Amateur Radio Operator, a Private Pilot, and a registered Professional Engineer in Texas.